Experimental Study on Optical Characterization of Mono Crystalline Silicon Solar Cell

A Thesis Submitted to the Institute of Energy in partial Fulfillment of the Requirement for the Degree of

Master of Science in Renewable Energy Technology

Institute of Energy, University of Dhaka

January 2016

A Thesis on

Experimental Study on Optical Characterization of Mono Crystalline Silicon Solar Cell

By

Nusrat Chowdhury

Examination Roll number: 424

Registration number:HA- 324

Admission session:2013-14

Supervisor's Declaration

The MS level research on "**Experimental Study on Optical Characterization of Mono Crystalline Silicon Solar Cell**" has been carried out and the dissertation was prepared under my direct supervision. Herby I confirm that, to the best of my knowledge the thesis represents the original research work of the candidate; the contribution made to the research by me, by others of the University was consistent with normal supervisory practice, and external contributions to the research are acknowledged.

I believe the thesis to be in a suitable presentational form and is ready for examination.

Dr. Zahid Hasan Mahmood
Professor
Department of EEE,
University of Dhaka
Dhaka, Bangladesh

Date: _____

Candidate's Declaration

I confirm that this thesis represents my own work; the contribution of any supervisors and others to the research and to the thesis was consistent with normal supervisory practice. External contributions to the research are acknowledged.

Nusrat Chowdhury
MS student
Admission Session: 2013-2014
Institute of Energy, University of Dhaka
Dhaka, Bangladesh

Date: _____

Acknowledgements

At first, all my credit and gratitude goes to our Almighty Allah. Without Whose Blessings it is impossible to finish my work properly.

I am deeply thankful to my supervisor professor Dr. Zahid Hasan Mahmood for overall guidance and encouragement to take up this thesis. I am also thankful to the director of Institute of Energy, Dr. Saiful Huque for his technical support in completing the work.

I am obliged to Md. Abdur Rafiq Akand, Senior Scientific Officer & Head of Institute of Electronics in Atomic Energy Research Establishment (AERE) for allowing me to get involved with the Solar Cell and Fabrication Division and carry out my thesis. And I am extremely grateful to him for being my co-supervisor and guiding me with his ideas, advice and assistance. Without his and Ms. Nahid Akter's continuous support and guidance the completion of thesis would not have been possible.

I also express my gratitude to Dhaka University for giving me the opportunity of availing its resources and enhancing my knowledge. I am also grateful to our teachers, fellow classmates, friends for their constant support to continue with this work. We would also like to thank our parents for their understanding and bearing with us for the whole period of this task.

Abstract

The experimental works have been done on the optical characterization of mono crystalline solar cell by Surface Photo Voltage (SPV) measurement for fabricated solar cell by observing minority carrier diffusion length (L) & life time (τ). The core objective of this research was to reduce the cost of solar cell and increase the efficiency by analysis the optical characterization. As the PV cell is one kind of photo diode so the surface photo voltage is very important part of characterization of cell fabrication. There is a direct relation between the minority carrier lifetime and solar cell efficiency. The method of SPV is a contactless system that helps to analysis the optical characterization of semiconductors. It measures the diffusion length of minority carriers in the region of essential light absorption inside solar cells and wafers. The minority carrier diffusion length, L is an important factor for cell efficiency and spectral response of the mono crystalline silicon solar cell. It is also necessary for evaluation of the p-type silicon wafer. In this experiment the surface photo voltage (SPV) of fabricated solar cells have been analyzed and observed minority carrier flow by Light Current Voltage (LIV) tester as it represented the quality of fabrication process and efficiency of the solar cell. A simple computer-controlled, normal incidence measurement system was designed for SPV measurements of minority carrier diffusion length and lifetime of Si-solar cell. Measurement system is based on a mini monochromator driven with a steeper motor to vary wavelengths in 400-1200 nm spectral range . Light induced surface photo voltage is measured as a function of the wavelength. SPV is measured using a Standard Research 510 lock in amplifier. A LabVIEW interface is used for system control and data acquisition. After calculating the experimental data obtained from mono crystalline silicon solar cells measurement, minority carrier diffusion length and life time were calculated and it was 92 μm and almost 3.135 μs respectively. By using solar simulator's (Sun Simulator K3000 LAB55) platform at 25^{o}C efficiency was measured and it was 16.04%.

TABLE OF CONTENTS

SUPERVISOR'S DECLARATION I
CANDIDATE'S DECLARATION II
ACKNOWLEDGEMENTS III
ABSTRACT IV
LIST OF FIGURES VIII

CHAPTER 1 1

INTRODUCTION 1
1.1. Background 1
1.2. Growth Rate Report of Renewable Energy in Global Aspects 2
1.2.1. Present Scenario of Power Crisis in Bangladesh 5
1.3. History of Solar Photovoltaic System 7
1.4. Principle of Operation of Solar Energy 8
1.4.1. Light Generated Current in a Solar Cell 9
1.4.2. Carrier Collection Probability of a Solar Cell 10
1.4.3. Quantum Efficiency of a Solar Cell 10
1.5. Advantages and Limitations of Solar Energy 11
1.6. Generation of Solar Photovoltaic Technologies 12
1.6.1. Crystalline Technology 12
1.6.1.1. Monocrystalline Silicon 12
1.6.1.2. Benefits of Monocrystalline Solar Cell 13
i. Longevity 13
ii. Efficiency 13
1.6.1.3. Limitations of Monocrystalline Solar Cell 14
1.6.2. Thin-film Technologies 15
1.7. objectives of this Thesis 16
1.8. Organization of this Thesis 16
REFERENCES 17

CHAPTER 2 19

SILICON MATERIAL FOR PHOTOVOLTAIC 19
2.1. Introduction 19
2.2. Doping 24
2.2.1. P-type Semiconductor 24
2.2.2. N-type Semiconductor 25
2.3. Orientation of Monocrystalline Silicon 25
2.4. P-N Junction for diode and solar cell 26
2.5. Parameters for Efficiency Test 29
2.5.1. I-V Curve 29

2.5.2. Short-Circuit Current 30
2.5.3. Open-Circuit Voltage 31
2.5.4. Fill Factor 31
2.5.5. Efficiency 32
2.6. Effect of few parameters 32
2.6.1. Characteristic Resistance 32
2.6.2. Effect of Parasitic Resistances 33
2.6.2.1. Series Resistance 34
2.6.2.2. Shunt Resistance 35
2.7. Effect of Temperature 36
2.8. Effect of Light Intensity 37
REFERENCE 38

CHAPTER 3 39

MONOCRYSTALLINE SOLAR CELL FABRICATION 39
3.1. Introduction 39
3.2. Fabrication Steps 40
3.2.1. Test Incoming Wafer 40
3.2.2. Saw Damage Removal 40
3.2.3. Hydrophobic Process 41
3.2.4. Surface Texturing Process 42
3.2.4.1. Result 44
3.2.5. Phosphorus Diffusion Process 44
3.2.6 Edge Isolation 46
3.2.7 Back and front contact /surface metallization 47
3.2.8 Co-firing by Rapid Thermal Annealing 48
REFERENCES 49

CHAPTER 4 52

MONOCRYSTALLINE SOLAR CELL CHARACTERIZATION 52
4.1. Characterization processes 52
4.2. Surface Reflection and Response (SRR) Method 52
4.3. Scanning Electron Microscope Analysis 54
4.4. Light-Current-Voltage (LIV) Tester 55
4.5. Surface Photovoltage (SPV) Method 56
4.6. Four Point Probe 58
4.6.1. The Measurement of Bulk Resistivity 60
4.6.2. Measuring Shunt Resistance (R_{SH}) and Series Resistance (R_S) from I_V Characteristics Curve 60
REFERENCES 62

CHAPTER 5 63

RESULT AND ANALYSIS 63

PART A 63
5.1. Solar Photovoltage (SPV) Measurement 63
5.2. SPV Method Description 63
5.3. Minority Carrier Diffusion Length & Lifetime 64
5.4. Experimental SPV Setup 66
5.4.1. Mini Mono-Chromator 67
5.4.2. Stepper Motor 68
5.4.3. SR510Lock-in Amplifier 69
5.4.4. Light chopper 71
5.4.5. ITO/Au Coated Quartz Plate 72
5.4.6. Setup Procedure on Computer Data Acquisition 73
5.5. Experimental Results 76
5.6. Discussion 79
PART B 79
5.7. Efficiency Measurement and I-V Characteristic 79
5.8. Experimental Setup for Efficiency Measurement 80
5.8.1. Specification of Reference Cell (K801) 81
5.9. Equation for Measuring the Solar Cell Efficiency 81
5.10. Experimental Result 82
5.11. Discussion 84
REFERENCES 85
CHAPTER 6 86
CONCLUSION 86
APPENDIX 87
APPENDIX 1 87
SUN SIMULATOR 87
APPENDIX-2 89
SPECIFICATION FOR K730 SOLAR CELL I-V TEST SOFTWARE 89
APPENDIX-3 90
1. MATHLAB CODE FOR SPV CURVE 90
2. MATLAB CODE FOR I-V CHARACTERISTIC CURVE 91

LIST OF FIGURES

Figure 1.1. Estimated Renewable Energy 3
Figure 1.2.Growth rate of Renewable 4
Figure 1.3.Cross section of a solar cell 8
Figure 1.4. Silicon Solar Cell and its working mechanism 9
Figure 1.5. The quantum efficiency of silicon 11
Figure 1.6. Mono crystalline silicon solar cell 13
Figure 2.1. The periodic table of the element. 19
Figure 2.2.The solar spectrum at AM1.5. 22
Figure 2.3.Three basic bond pictures of a semiconductor. (a) Intrinsic Si with no impurity. 25
(b) n-type Si with donor (phosphorus). (c) p-type Si with acceptor (boron). 25
Figure 2.4. Crystal orientation of monocrystalline silicon 26
Figure 2.5.Charge carrier distribution at p-n junction and currents through the junction 27
Figure 2.5. I-V Characteristics curve of an ideal p-n junction diode 28
Figure 2.6.The effect of light on the current-voltage Characteristics of a p-n junction 30
Figure 2.7. I - V curve of a solar cell showing the short-circuit current, open-circuit Voltage, fill factor 'FF', maximum power point (Vmp, Imp) 31
Figure 2.8. The characteristic resistance of a solar cell 33
Figure 2.9. Parasitic resistances in a solar cell circuit 34
Figure 2.10. I-V curve for different series resistances 35
Figure 2.11. I-V curve for different parallel resistances 36
Figure 2.12. Effect of temperature on the IV characteristics of a solar cell 37
Figure 3.2.RCA cleaning process: DI water dip(left),cleaning process: Nitric Acid solution(Right) 41
Figure 3.3. Comparison of SEM image of the (a) raw wafer and (b) saw damage removed wafer 42
Figure 3.4. After Clean Wafers in Texturing process 43
Figure 3.5. Compress air gun for wafer drying 43
Figure 3.6. SEM of the p-type textured silicon wafer 44
Figure 3.7. The phosphorus doped silicon wafer 46
Figure 3.8. (a) Screen printer (b) screen printing frame 47
Figure 3.10. a) Microscopic image of the screen b) Image of front side printing mask 48
Figure 3.11. Contact firing at RTC furnace 48
Figure 4.1. Schematic diagram of the surface reflection and measurement system 53
Figure 4.2.Picture of surface reflection 54
Figure 4.3.(a)Scanning electron microscope (b), SEM image of randomly textured 55
Figure 4.4. LIV measurement System. 56

Figure 4.5. SPV Signal Changes with Penetration of incident light and wavelength.....57
Figure 4.6. SPV Measurement System.....58
Figure 4.7. Resistance measurement by Four Point Probe.....59
Figure 4.8. Four Point Probe 59
Figure 4.9. Effect of Diverging Rs & RSH from Ideality 61
Figure 4.10. Obtaining Resistances from the I-V Curve.....61
Figure 5.1. Change in surface potential without (a) and with light illumination (b) 64
Figure 5.2. Basic block diagram of the SPV measurement.....67
Figure 5.3. Close-up views of the SPV system showing wafer chuck, interface box, and the folding mirror 68
Figure 5.4. 150W fibre optical microscopic illuminator, Motorized monochromator,.....68
Figure 5.5. Stanford research 510 lock-in amplifier. 70
Table 5.1. Specification of Lock in Amplifier.....71
Table 5.2. Specification of Light chopper.....71
Figure 5.6. The wafer under test sandwiched between the Au-coated chuck and ITO-coated quartz plate with Au-coated contacts at boundaries (right).....72
Figure 5.7. Close-up views of the contact for Au/ITO-coated quartz plate (left).....73
Figure 5.8. Working SPV system with lock-in exhibiting signal of 0.74 and frequency of 146 Hz. 73
Figure 5.9. The form of graph displayed, where λ-SPV is plotted. 75
Figure 5.10. The ideal form of penetration depth versus 1/Vspv graph that is plotted with the help of data in Fig. 5.9. 75
Figure 5.11. The LabVIEW Image 77
Figure 5.12. 1/alpha vs 1/Vspv represents minority carrier diffusion length.....78
Figure 5.13. Complete setup of the system. 80
Table 5.2 Specification of Reference Cell (K801).....81
Table 5.5. Results from sun simulator 83
Figure 5.16. 1 I-V Characteristics Curve of Sample Solar Cell 84

LIST OF TABLES

Table2.1. Properties of a Silicon Material……..……02
Table 5.1. Specification of Lock in Amplifier ……71
Table 5.2. Specification of Light chopper……..……. 71
Table 5.3. Data obtained from the SPV measurement system…….…....76
Table:5.4. Specification of Reference Cell(K801)……..…….. 81
Table 5.5. Results from sun simulator……..… 83

Chapter 1

Introduction

1.1.Background

At present energy crisis is one of the major concern that the world's facing due to the limited natural resources that are used to power industrial society are diminishing as the demand rises. These natural resources are in limited supply. So every government's and concerned individuals are working to make the most efficient use of renewable resources a priority. In Southeast Asia shortage of power system is prevailing. There is always remaining a gap of 1000-1500MW between generated power and demanded power [1]. The main reason of energy crisis is caused by poor efficiency of power generating equipments and the lack of sufficient energy storage.

Carbon based fuel creates most of its energy such as electricity through burning. This energy generation process leaves harmful impact for the earth. As early as the 16^{th} century, environmental impact of burning fossil fuels was considered. Burning of fossil fuel leads to accumulation of sulfur dioxide (SO_2) and other harmful gases in the atmosphere. In addition, the burning process enhances the carbon dioxide (CO_2) concentration in the atmosphere. Carbon dioxide is also known as green house gas. According to Canadian Energy Research Institute report, burning fossil fuel globally produce 6.3 billion metric tons of carbon dioxide per year(World Energy: The past and Possible Futures). Since, the Earth's atmosphere can only absorb half of this amount; the rest contributes to the global warming. It is estimated that one ton of Carbon dioxide contributes to $1.5x10^{-12}$ degrees of global temperature change (Science Daily, 2011).

In addition to the environmental effects of burning fossil fuel, we also face depletion of fossil fuels. Fossil fuel is non-renewable energy resource. The gap between the energy demand and its production from fossil fuels is widening. The most obvious consequence is the increase in fuel prices. Increasing fuel price leads to increase in the cost of living and daily expenses.

Therefore, there is an urgent need to find an alternative energy resource to fulfill the global energy requirements. The alternate energy resource that meets the requirement of sustainable, cyclic, environmental friendly, carbon free, chemical free, clean and inexpensive is in the form

of a renewable energy resource. The earth needs a safe and long lasting energy resource. Unless we give renewable energy a serious thought, the problem of energy crisis cannot be solved easily. Renewable energy sources like- solar, wind or combination of both can reduce our dependency on fossil fuels and also helps to reduce greenhouse gas emission. For Bangladesh, solar is the best renewable source as a coastal zone. Solar energy is the direct conversion of sunlight using PV panel. But unfortunately our country doesn't produce equipments for PV panels. We import PV cell mostly from European countries. But the efficiency of these is very poor. Although one of the most costly parts of solar installation covers the storage but if we focus on direct grid supply concept then the efficiency of the panel will put a huge cost efficient factor for the whole system. On the other hand, if we replace the existing PV panel with the efficient one then the life time of the system will be increased and the system will be more efficient than before.

To increase the efficiency of solar cell, we need to analysis the fabrication and characterization process of PV cell. The aim of this work is to analysis the optical characterization of mono crystalline solar cell by Surface Photo Voltage (SPV) measurement for fabricated solar cell by observing minority carrier diffusion length & life time and also Light-Current-Voltage (LIV) testing is done to evaluate the performance of the cell and mainly to calculate the efficiency of the solar cell. The main objective of this research is to reduce the cost of solar cell and increase the efficiency by analysis the optical characterization.

1.2. Growth Rate Report of Renewable Energy in Global Aspects

Renewable energy continued to grow in 2014 against the backdrop of increasing global energy consumption and a dramatic decline in oil prices during the second half of the year [2]. Global final energy consumption has increased by about 1.5% annually in recent years, driven primarily by rising demand in developing countries [3].

Despite rising energy use, for the first time in four decades, global carbon emissions associated with energy consumption remained stable in 2014 while the global economy grew [4]. Whereas previous emissions decreases were associated with downturns in the global economy, the carbon stabilization in 2014 has been attributed to increased penetration of renewable energy and

improvements in energy efficiency [4]. Several countries—including China, Mexico, and the United States—as well as the European Union have announced climate change commitments that set the stage for future investment in renewable and energy efficiency [4].

There is rising awareness worldwide that renewable energy and energy efficiency are critical not only for addressing climate change, but also for creating new economic opportunities, and for providing energy access to the billions of people still living without modern energy services. Renewable are vital elements of rural electrification programs in many countries, and dozens of international actors were involved in advancing energy access through renewable during 2014 [5].

According to the data by 2013, renewable energy provided an estimated 19.1% of global final energy consumption. Of this total share, traditional biomass, used primarily for cooking and heating in remote and rural areas of developing countries, accounted for about 9%, and modern renewables increased their share slightly over 2012 to approximately 10.1% [5].

Modern renewable energy is being used increasingly in four distinct markets: power generation, heating and cooling, transport, and rural/off-grid energy services. In 2013, hydropower accounted for an estimated 3.9% of final energy consumption; other renewable power sources comprised 1.3%; renewable heat energy accounted for approximately 4.1%; and transport biofuels provided about 0.8% [5].

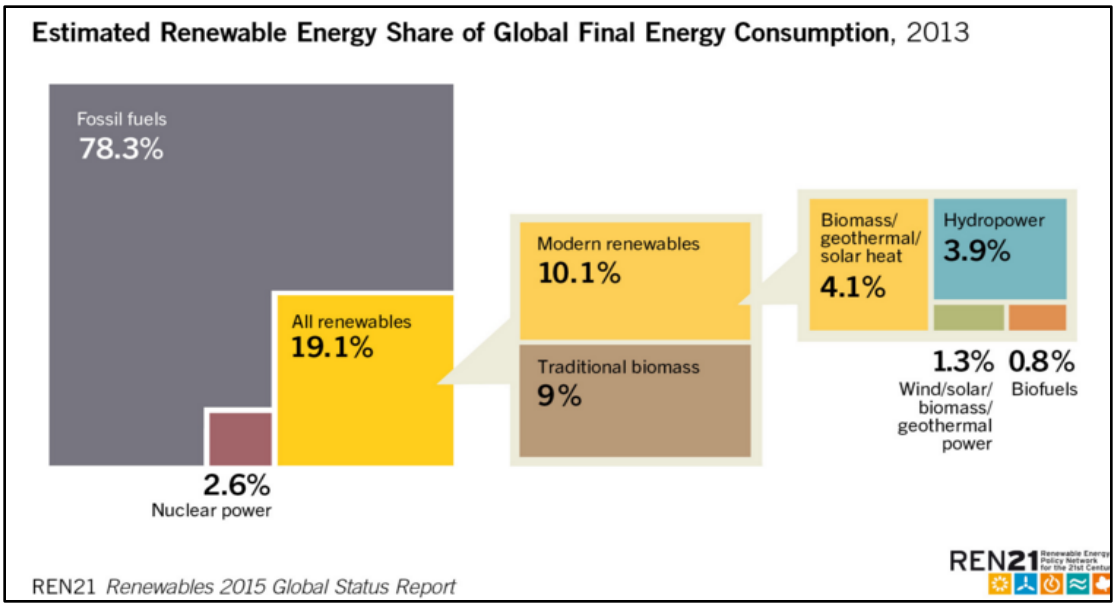

Figure 1.1. Estimated Renewable Energy [5]

In 2014, renewable energy overall expanded significantly in terms of capacity installed and energy produced. Some technologies experienced more rapid growth in deployment in 2014 than they have averaged over the past five years [5]. The most rapid growth, and the largest increase in capacity, occurred in the power sector.

Growth is also driven by the increasing cost-competiveness of renewable energy. Renewable energy costs continued to decline in 2014, and in many countries renewable are broadly competitive with conventional energy sources. In terms of cost and environmental performance, distributed renewable systems also are competitive with fossil fuels (especially diesel) for heat and electricity in islands and remote jurisdictions, and, in general, for providing access to modern energy services [5]. In remote and rural areas of developing countries—and increasingly deployed to power mini- and micro-grids—renewable are playing a large and growing role in providing essential and productive energy services, due largely to growing recognition of their cost-effectiveness.

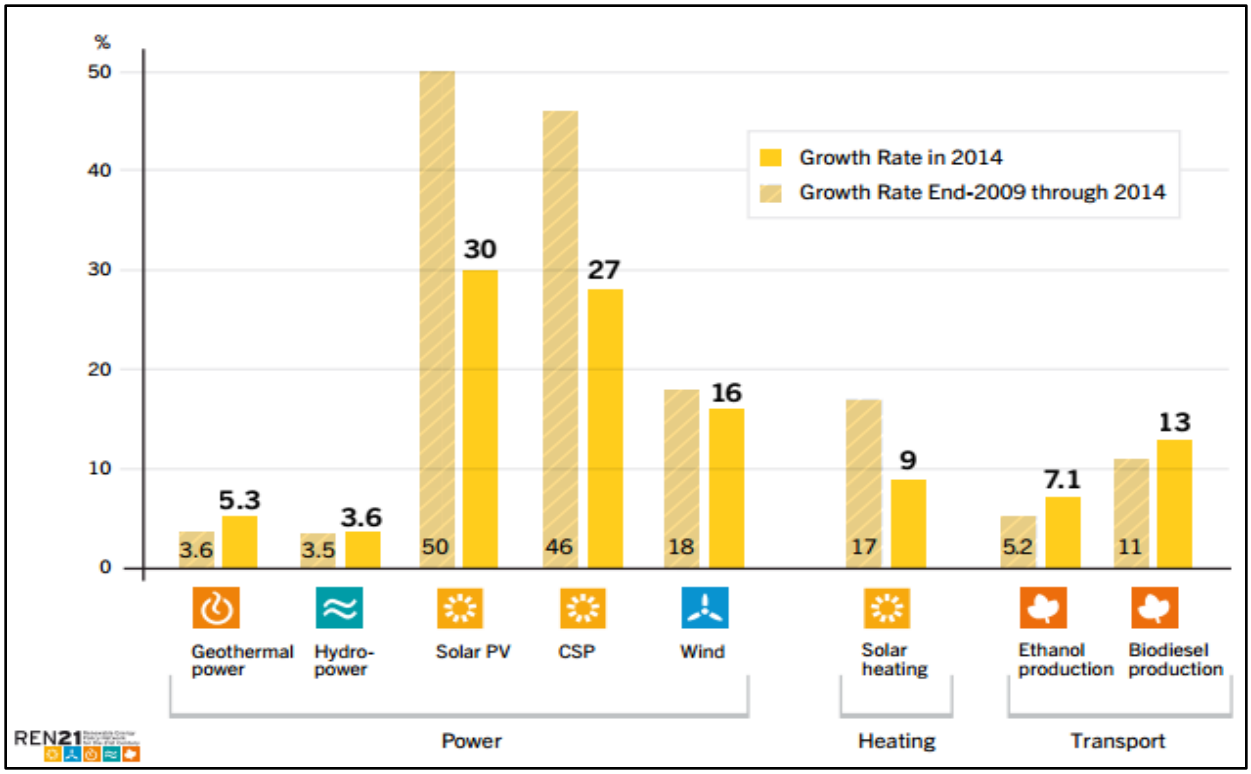

Figure 1.2.Growth rate of Renewable [5]

1.2.1. Present Scenario of Power Crisis in Bangladesh

Bangladesh has been facing a severe power crisis in the recent years. Power generation in the country is almost entirely dependent on natural gas, which accounts for 81.4% of the electricity generation of the total installed capacity 12,071 MW. At the current rate of increase in consumption (10% annually), the national proven reserve of natural gas may not last more than 15-20 years. Only limited amount of coal resource is available to generate electricity, although it has adverse environmental impact. On the other hand, the government of Bangladesh has declared that it aims to provide electricity for all by the year 2020, although at present there is a high unsatisfactory demand for energy, which is growing by more than 8% annually. The Rural Electrification Board (REB) in its master plan of 2000 noted that it had supplied electricity services to about 31% of the total rural population. It aims to reach 97 million rural populations by 2020, which is about 84% of the total rural population. In order to meet this target only fossil fuel based power plant would not be able to satisfy the demand. It needs to look for the alternative sources of energy for power generation.

Renewable energy technologies would be one of the important emerging options. Bangladesh is situated between 20.30 and 26.38 degrees north latitude and 88.04 and 92.44 degrees east longitude, which is an ideal location for solar energy utilization. Daily solar radiation varies between 4 and 6.5 kWh/m^2. Solar PV technology is an important emerging option for electricity generation. So, densely populated tropical country like Bangladesh could be electrified by PV grid system using the inexhaustible and pollution free solar energy without using any novel technologies. Compensation of electricity shortage and reduction CO2 emission would be done by introducing solar energy sources for electricity generation in mass scale [6].

Solar energy can be used to pull the country from the quagmire of energy crisis. This energy is available throughout the whole country and it does not demand strong industrial base to harness it. Altogether, solar energy has the promise and potential of solving Bangladesh's energy problem.

Bangladesh has 15 MW solar energy capacities through rural households and 1.9 MW wind power in Kutubdia and Feni. Bangladesh has planned to produce 5% of total power generation by 2015 & 10% by 2020 from renewable energy sources like air, waste & solar energy [7].

Bangladesh is set to install 2,000 photovoltaic mini-grid power plants by 2014 in a bid to bring its off-grid areas under the power network. Many Infrastructure Development Companies have reportedly said they will provide loans for the project. As part of the new generation expansion initiative in line with growing demand, Government has plan to enhance national power generation capacity to be 16000 MW by 2015. Expected generation from renewable sources should be then at least 800 MW as envisioned in National Renewable Energy Policy. However, estimated output per unit of renewable energy based installed capacity is far less than conventional power plants. Therefore, in order to achieve a dependable generation of 800 MW, installed capacity of renewable energy based power should be at least 1000-1200 MW. Moreover, considering a proven resources as of date, solar power should dominate in the renewable energy development initiative [8].

As of 2010, solar photovoltaic generates electricity in more than 100 countries and, while yet comprising a tiny fraction of the 4.8 TW total global power-generating capacities from all sources, is the fastest growing power-generation technology in the world. Between 2004 and 2009, grid-connected PV capacity increased at an annual average rate of 60 percent, to some 21 GW. Off-grid PV accounts for an additional 3–4 GW [9].Bangladesh has 80 MW solar energy capacities through rural households and 1.9 MW wind power in Kutubdia and Feni. Bangladesh has planned to produce 5% of total power generation by 2015 & 10% by 2020 from renewable energy sources like air, waste & solar energy [10].

Although Bangladesh boasts significant experience in installing solar home systems in remote and off-grid areas, the solar mini-grid project is the first of its kind here. As of May 2011, 950,000 plus photovoltaic systems were installed in Bangladesh, supported by the government and financed by many Infrastructure Development Company, along with 30 NGOs and private sector partners[7]. As another new addition to the energy sector, the Bangladesh Government recently has taken up a pilot project to use solar energy for irrigation pumps. The Bangladesh's government has also lifted all sorts of tax and VAT on renewable energy equipment to encourage the use of sustainable renewable energy sources [7].

1.3.History of Solar Photovoltaic System

The first person to observe the Photovoltaic Effect, in 1839, was French physicist Edmond Becquerel. He observed that voltage of a 'wet cell' battery increased when its silver plates were exposed to sunlight [11]. In 1861[8], Auguste Mouchet manufactured the first solar powered motor, which ran on steam. The first solar PV cells were made in the 1880's and had an efficiency of around 2% [11]. In 1877 two Cambridge scientists, W. G. Adams and R. E. Day discovered PV effects in a solid substance. 1883 Charles Edgar Fritts, a New York electrician, constructed a selenium solar cell that was in some respects similar to the silicon solar cells of today. Aubrey Eneas opened the first solar company in Boston, US, in 1900 and called it The Solar Motor Co. William J. Bailley invented a solar collector in 1908, which comprised of copper coils feeding an insulated box. This is very similar to the ones used today. A process used to make very pure crystalline silicon, known as the Czochralski meter, was developed in the early 1950's. In 1954, Bell Telephone Laboratories invented a 4% efficient photovoltaic solar panel, later improving it to 11% efficient. A small US satellite was powered by a cell producing less than one watt in 1958[11]. In 1962Bell Telephone Laboratories launches the first telecommunications satellite, the Telstar (initial power 14 watts). [11]In 1970, Elliot Burman developed solar cells which were significantly less costly, reducing the price from $100 to $20 per watt, and then in 1973/4 the oil embargo allowed the solar industry to grow, with the US Department of Energy funding the Federal Photovoltaic Utilization Program, allowing for the testing and installation of over 3000 PV systems. In 1976 David Carlson and Christopher Wronski, RCA Laboratories, fabricate first amorphous silicon photovoltaic cells. In 1994 The National Renewable Energy Laboratory develops a solar cell—made from gallium indium phosphide and gallium arsenide—that becomes the first one to exceed 30% conversion efficiency [12].

Approximately 1.2 billion homes were using Solar Geysers by the 1990's; it was becoming more and more popular. In 2005, thin film solar modules were invented by Professor Vivian Alberts of South Africa [11].

1.4.Principle of Operation of Solar Energy

A solar cell is an electronic device which directly converts sunlight into electricity. Light shining on the solar cell produces both a current and a voltage to generate electric power. This process requires firstly, a material in which the absorption of light raises an electron to a higher energy state, and secondly, the movement of this higher energy electron from the solar cell into an external circuit. The electron then dissipates its energy in the external circuit and returns to the solar cell. A variety of materials and processes can potentially satisfy the requirements for photovoltaic energy conversion, but in practice nearly all photovoltaic energy conversion uses semiconductor materials in the form of a p-n junction.

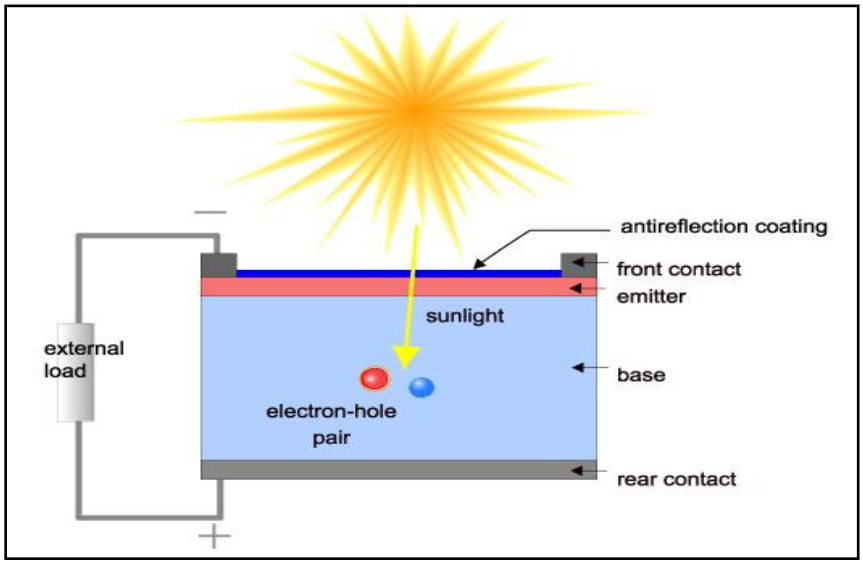

Figure 1.3.Cross section of a solar cell [14]

Solar cell converts photons in Solar rays to direct-current (DC) and voltage. The associated technology is called Solar Photovoltaic (SPV). A typical silicon PV cell is a thin wafer consisting of a very thin layer of phosphorous-doped (N-type) silicon on top of a thicker layer of boron-doped (P-type) silicon. An electrical field is created near the top surface of the cell where these two materials are in contact (the P-N junction).

When the sunlight hits the semiconductor surface, an electron springs up and is attracted towards the N-type semiconductor material. This will cause more negatives in the n-type and more

positives in the P-type semiconductors, generating a higher flow of electricity. This is known as Photovoltaic effect. Figure 1.4 below shows the working mechanism of a silicon solar cell.

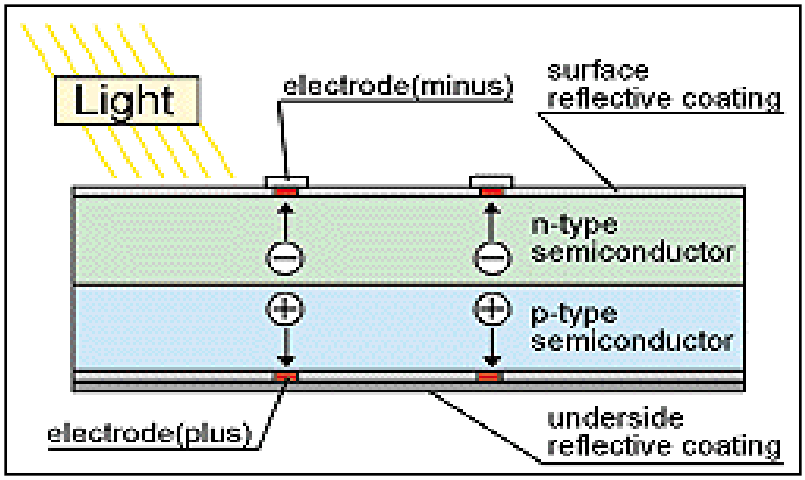

Figure 1.4. Silicon Solar Cell and its working mechanism [15]

The basic steps in the operation of a solar cell are:

- the generation of light-generated carriers
- the collection of the light-generated carries to generate a current
- the generation of a large voltage across the solar cell
- the dissipation of power in the load and in parasitic resistances

1.4.1. Light Generated Current in a Solar Cell

The generation of current in a solar cell, known as the "light-generated current" involves two key processes. The first process is the absorption of incident photons to create electron-hole pairs. Electron-hole pairs will be generated in the solar cell provided that the incident photon has energy greater than that of the band gap. However, electrons (in the p-type material), and holes (in the n-type material) are meta-stable and will only exist, on average, for a length of time equal to the minority carrier lifetime before they recombine. If the carrier recombines, then the light-generated electron-hole pair is lost and no current or power can be generated. A second process,

the collection of these carriers by the p-n junction, prevents this recombination by using a p-n junction to spatially separate the electron and the hole. The carriers are separated by the action of the electric field existing at the p-n junction. If the light-generated minority carrier reaches the P-n junction, it is swept across the junction by the electric field at the junction, where it is now a majority carrier. If the emitter and base of the solar cell are connected together the light-generated carriers flow through the external circuit.

1.4.2. Carrier Collection Probability of a Solar Cell

The collection probability describes the probability that a light generated carrier absorbed in a certain region of the device will be collected by the p-n junction and therefore contribute to the light-generated current, but probability depends on the distance that a light-generated carrier must travel compared to the diffusion length. Collection probability also depends on the surface properties of the device. The collection probability of carriers generated in the depletion region is unity as the electron-hole pair is quickly swept apart by the electric field and are collected. Away from the junction, the collection probability drops. If the carrier is generated more than a diffusion length away from the junction, then the collection probability of this carrier is quite low. Similarly, if the carrier is generated closer to a region such as a surface with higher recombination than the junction, then the carrier will recombine.

1.4.3. Quantum Efficiency of a Solar Cell

The quantum efficiency is the ratio of the number of carriers collected by the solar cell to the number of photons of a given energy incident on the solar cell. The quantum efficiency may be given either as a function of wavelength or as energy. If all photons of a certain wavelength are absorbed and the resulting minority carriers are collected, then the quantum efficiency at that particular wavelength is unity. The quantum efficiency for photons with energy below the band gap is zero. A quantum efficiency curve for an ideal solar cell is shown below.

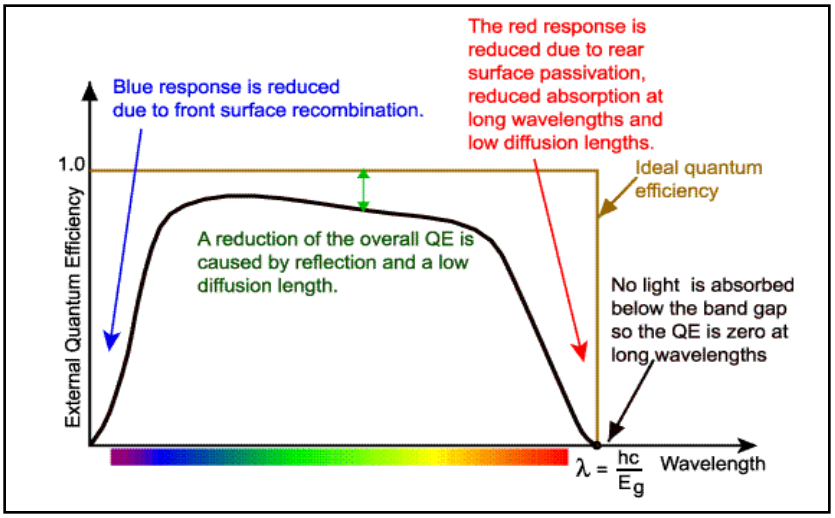

Figure 1.5. The quantum efficiency of silicon [15]

1.5.Advantages and Limitations of Solar Energy

Renewable energy sources in general, and Solar Energy source in particular, has the potential to provide energy services with zero or almost zero emission. The solar energy is abundant and no other source in renewable energy is like solar energy. Every technology has its own advantages and disadvantages. As the solar insolation and atmospheric conditions vary significantly from place to place, efficiency of solar energy also differs accordingly.

Advantages

- It is an abundant Renewable Energy technology.
- The technology led to development of stable solar cells with efficiency 25%.
- Two types of crystalline silicon are used in the industry. They are Monocrystalline Silicon.
- This technology is Omni present and it can be captured for conversion on a daily basis.
- It is a Non-polluting technology, which means that it does not release green house gases
- It is a Noiseless technology as there are no moving parts involved in energy generation
- This technology requires Low-maintenance because of lack of moving parts
- It can be installed on modular basis and expanded over a period of time

- Most viable alternative for providing electricity in remote rural areas as it can be installed where the energy demand is high and can be expanded on modular basis.

Limitations

- As the technology is in an evolving stage, the efficiency levels of conversion from light to electricity is in the range of 10 to 17%, depending on the technology used.
- The initial investment cost of this technology is high. At present the technology is basically surviving because of subsidy schemes available by the government.
- As the efficiency levels are low, the space required is relatively high. For instance, with the existing levels of technologies, the land required for putting up a 1 MW solar PV power plant is between 6 to 9 acres. However, research is going on to increase the efficiency levels of the cell.
- Solar energy is heavily dependent on atmospheric conditions.

1.6. Generation of Solar Photovoltaic Technologies

Solar cell technologies differ from one another based firstly on the material used to make the solar cell and secondly based on the processing technology used to fabricate the solar cells. The material used to make the solar cell determines the basic properties of the solar cell, including the typical range of efficiencies.

1.6.1. Crystalline Technology

Crystalline Silicon (c-Si) was chosen as the first choice for solar cells, since this material formed the foundation for all advances in semiconductor.
Two types of crystalline silicon are used in the industry. They are
• Monocrystalline Silicon
• Multicrystalline Silicon

1.6.1.1. Monocrystalline Silicon

Mono-Crystalline Silicon cells are produced by growing high purity, single crystal Si rods and slicing them into thin wafers. Single crystal wafer cells are expensive. They are cut from

cylindrical ingots and do not completely cover a square solar module. This results in substantial waste of refined silicon. The efficiency of mono-crystalline silicon cells generally remains between 17-18% because of the purity level.

Figure 1.6. Mono crystalline silicon solar cell

1.6.1.2. Benefits of Monocrystalline Solar Cell

Monocrystalline Solar cells are the oldest solar cell. There are many advantages of monocrystalline silicon solar cell compare to other cells.

i. Longevity

Monocrystalline solar cells are first generation solar technology and have been around a long time, providing evidence of their durability and longevity. This type of solar cell can last a long time, there will come a time when the lower efficiency makes it economically desirable to replace the panels especially as the efficiency of newer panels continues to increase.

ii. Efficiency

As already mentioned, PV panels made from monocrystalline solar cells are able to convert the highest amount of solar energy into electricity of any type of flat solar panel. Consequently, if your goal is to produce the most electricity from a specific area (e.g., on a roof) this type of panel should certainly be considered.

Consequently, Monocrystalline panels are a great choice for urban settings or where space is limited. As a developer of PV rooftop installations in Germany, buying or leasing roof space is a significant cost of the whole project and so you want to be able to produce as much electricity you can from this valuable resource.

iii. Lower Installation Costs

The cost of solar panels is typically around 60% of the cost of a fully installed solar power system, with installation being a significant cost component.

iv. Other Environmental Concerns

Some thin film solar products uses cadmium telluride (CdTe) . Cadmium is a heavy metal that accumulates in plant and animal tissues. Cadmium is a 'probable carcinogen' in humans and animals. While cadmium telluride doesn't pose a threat while the panel is in service, disposal of this toxic waste when the product reaches the end of its life comes an at large cost and suitable facility which is why firms like First Solar offer their own "end of life" recycling program to take care of disposing this material. Monocrsytalline solar panels are not hazardous to the environment.

v. Greater Heat Resistance

Like other types of solar cell, monocrystalline solar cells suffer a reduction in output once the temperature from the sunlight reaches around fifty degrees Celsius/a hundred and fifteen degrees Fahrenheit. Reductions of between twelve and fifteen percent can be expected. This loss of efficiency is lower than the polycrystalline cells.

There are so many advantages of Monocrystalline silicon solar cell. For that reason I choose Monocrystalline Silicon for my thesis.

1.6.1.3. Limitations of Monocrystalline Solar Cell

The initial investment cost of this technology is high and the efficiency is still very poor.

1.6.2. Thin-film Technologies

The manufacturing process of thin-film modules is quite different from that of the c-Si ones. Instead of making separate wafers, the semiconductor materials used in thin-film photovoltaics are deposited in gaseous form onto glass or metal substrates. The whole module is made in one time: To the glass super strate first a transparent conductor and long metal bars that connect the adjacent cells are attached. Subsequently the different semiconductor layers are deposited in gaseous form, and finally the bottom conductor is attached. The straightforward manufacturing process makes thin-film module especially suitable for mass production, which naturally brings their costs down [16].

As the layer of the photovoltaic material is very thin in thin-film modules less photons are absorbed, and part of the light passes right through. This results in smaller efficiency as compared to c-Si modules, but also opens up new opportunities. First of all, the semi-transparent photovoltaic material can be deposited on glass to make windows that also produce electricity.

Secondly, thin-film materials can be used to produce highly efficient multiple junction solar cells, where two or more junctions with different band gaps are stacked on top of each other. The multijunction solar cells are constructed so that the uppermost layer exploits the shortest wavelengths (highest-energy photons) and the lowermost exploits the longest wavelengths. This is done by choosing semiconductor materials with higher band gaps to the uppermost layer, and materials with lower band gaps into the subsequent layers in descending order [16].

Most of the thin-film modules are currently made of amorphous silicon (a-Si), but also different compounds are used: Gallium Arsenide (GaAs), Cadmium Telluride (CdTe) and Copper Inidium Diselenide (CIS). Amorphous silicon, that is silicon with very little order in the atomic arrangement, has the advantage of the good availability of silicon. It is also very suitable for production of multijunction modules. However, the problem with a-Si modules is that their performance degrades significantly during the first months of operation: commercial modules have stabilized efficiencies of only 5-8%, though in laboratories stabilized efficiency of 13% have been reached. The advantage of GaAs and CdTe is their close-to optimal band gaps, 1.43 eV for GaAs and 1.44 eV for CdTe, resulting in relatively high efficiency. But these materials

are not trouble-free either: gallium is a rarer element than silicon, which lifts its costs, and cadmium in turn is highly toxic, which causes safety problems in both manufacturing and usage of CdTe modules. The highest efficiencies so far among single-junction thin-films at both laboratories and industrial scale have been reached with CIS cells and modules [10]. Furthermore, the homogenous and opaque appearance of CIS modules renders them especially suitable for building integration of PV modules, which offers new opportunities for popularization of photovoltaics [17] [16].

The multijunction technology is also promising, and very high efficiencies have been reached with it. With multijunction GaAs-GaInP (Gallium Inidium Phosphorus) solar cells, 29.5% efficiency have been reached and these cells are used in space applications and for concentrator PV. For multijunction a-Si, the theoretical upper limit for the efficiency is 42% and for modules in laboratories stabilized efficiencies of 11% have been reached [16].

1.7. objectives of this Thesis

The main objective of this research is to reduce the cost of solar cell and increase the efficiency by analysis the optical characterization. As the PV cell is one kind of photo diode so the surface photo voltage is very important part of characterization of cell fabrication. There is a direct relation between the minority carrier lifetime and solar cell efficiency. The SPV method is a well-established contactless technique for the characterization of semiconductors, namely for measurement of diffusion length of minority carriers in the region of essential light absorption inside solar cells and wafers. The aim of this work is to analysis the optical characterization of mono crystalline solar cell by Surface Photo Voltage (SPV) measurement for fabricated solar cell by observing minority carrier diffusion length & life time and also sun simulator testing is done to evaluate the performance of the cell and mainly to calculate the efficiency of the solar cell.

1.8. Organization of this Thesis

In Chapter 2: Basic Semiconductor Properties and Physics: This chapter discuss about the basic semiconductor properties and its application in solar cell. Also, all the properties and parameters of solar cell are briefly discussed.

In Chapter 3: Monocrystalline Solar Cell Fabrication: In this Chapter standard fabrication process of monocrystalline silicon solar cell has been discussed in details and explains how p-n junction is formed from p-type wafer. Also explain the requirements of preparing solar cell that can produce more electricity.

In Chapter 4: Monocrystalline Solar Cell Characterization: All the techniques of optical characterization of monocrystalline solar cell is described in details. How this characterization helps to analysis the cell performance hence helps to increase the quality of a solar cell has been described in this chapter.

In Chapter 5: Result and Analysis: Optical Characterization has been analyzed for sampled solar cell. Also all the experimental criteria are explained in this chapter. A simple computer-controlled, normal incidence measurement system was designed for SPV measurements of minority carrier diffusion length and lifetime of Si-solar cell. Measurement system is based on a mini monochromator driven with a steeper motor to vary wavelengths in 400-1200 nm spectral range and solar simulator's (Sun Simulator K3000 LAB55) have been used for analysis efficiency, fill factor ,parasitic resistance and other important parameters.

In Chapter 6: Conclusion, discuss about the result and limitation and future scope.

References

[1] New Energy Foundation website.[Online]. [Cited December 1,2015] Available: http://www.nef.or.jp

[2]U.S. Energy Information Administration (EIA), "Short-term Energy Outlook: Global Crude Oil Prices," 12 May 2015, http:// www.eia.gov/forecasts/steo/report/prices.cfm

[3] Growth in final energy consumption for years 2007 through 2012, from International Energy Agency (IEA), World Energy Statistics and Balances, 2014 edition (Paris: OECD/IEA, 2014).

[4] Carbon emissions remained stable in 2014 compared to 2013, while the global economy grew by 3%. IEA, "Global Energy-related Emissions of Carbon Dioxide Stalled in 2014," 13 March 2015, http://www.iea.org/newsroomandevents/news/2015/march/ global-emissions-of-carbon-dioxide-stalled-in-2014.html

[5]Renewable Energy Policy network for the 21st century, "RENEWABLES 2015 GLOBAL STATUS REPORT", (cited 1 January 2016) available: http://www.ren21.net/wpcontent/uploads/2015/07/GSR2015_KeyFindings_lowres.pdf

[6] Md. Alam Hossain Mondal, A. K. M. Sadrul Islam" Techno-economic Feasibility of Grid Connected Solar PV System in Bangladesh".

[7] PV-Magazine website. Available: http://www.pv-magazine.com/news/details/beitrag/bangladesh-set-to-install-2-000-pv-power-plants_100003310

[8]Power Division Board Website.Available: http://www.powerdivision.gov.bd/index.php?page_id=262 (Cited:15January, 2016)

[9]en.wikipedia.org/wiki/Photovoltaics

[10] en.wikipedia.org/wiki/Electricity_sector_in_Bangladesh

[11] http://www.solarpowerstore.co.za/articles/history-of-solar-energy.html ; (Cited: January 4, 2015)

[12] inventors.about.com/od/pstartinventions/a/Photovoltics

[13]PV education website, Available: http://PVeducation.org/PVcdrom/solar-celloperation/solar-cell-structure

[14] Available: http://global.kyocera.com/prdct/solar/spirit/about_solar/cell.html

[15]http://PVeducation.org/PVcdrom/solar-cell-operation/quantum-efficiency

[16] G. M. Masters. Renewable and Efficient Electric Power Systems. JohnWiley & Sons, 2004.

[17] A. Virtuani, W. Zaaiman, and H. M¨ullejans, "Modified Visual Appearanceof Cu(In,Ga)(Se,S)$_2$ Thin Film Solar Modules for Building Integrated Photovoltaics"European Photovoltaic Solar Energy Conference (EU PVSEC), Milan, Italy, 2007.

Chapter 2

Silicon material for photovoltaic

2.1.Introduction

Silicon is a semiconductor material which is the second most abundant element (Clarke number ~26%) on Earth and exists mainly in the oxidized silicate (SiO2) form. Si sources are neither localized in very specific regions nor are they noble. However, crystalline silicons (c-Si) and amorphous (a-Si) silicons remain the most fundamental, purely inorganic materials used for microelectronics, optoelectronics, photonics and solar cells.

silicon is a group IV element in the periodic table of elements (see figure 2.1). This means that it has four electrons in its outermost shell, i.e., it has four valence electrons, which determines its electrical properties. Another common semiconductor is germanium that is also a group IV element. Compounds of elements for instance from groups III and V (gallium and arsenic), II and VI (cadmium and tellurium) and even I, III and VI (copper, indium and selenide) are also used to produce semiconductors [1].

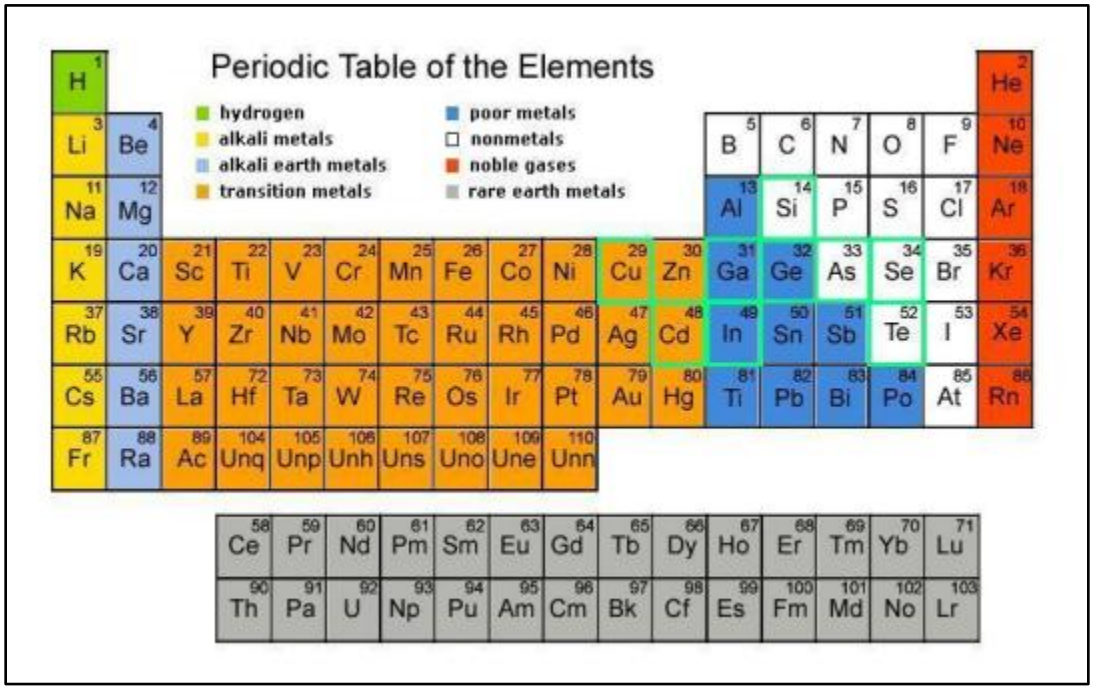

Figure 2.1. The periodic table of the element. [2]

Semiconductors, and elements used as compounds to produce semiconductors, are highlighted with green in figure 2.1[2].

In pure silicon crystal, the four valence electrons of a silicon atom are tied with strong covalent bonds to four adjacent silicon atoms. Therefore at zero temperature silicon is a perfect insulator there are no free electrons to carry currents as there are in metals, but all the electrons are tied to their nuclei. As the temperature increases, some electrons gain enough energy to escape from the potential field of their nuclei and thus the conductivity of silicon increases.

According to quantum mechanics, electrons in atoms have well-defined possible, discrete energy levels. As several atoms are brought into contact these levels spread out into so called bands. Depending on the distance of the atoms and the bonds between them, there might be bands of forbidden energy called band gaps between the atoms, or the bands may overlap, forming a continuum of allowed energy states in the material. The characteristics of insulators, conductors and semiconductors depend on their band structure. [3]

The bands of interest are the valence band, that is the highest completely filled band, and the conduction band. In the valence band all the energy states are occupied and hence its electrons are immobile, whereas in the conduction band there are plenty of unoccupied states for electrons to move in response to an applied electric field. To get to the conduction band, however, an electron has to jump over a gap – the forbidden band between the valence and conduction bands. Hence the conductivity properties of a material are dependent on the size of this gap, called the band gap energy. In conductors the valence and conduction bands overlap; thus there is lots of mobile electrons to carry a current already at lower temperatures. In insulators, the band gap energy at room temperature can be 5 eV or more, and in semiconductors it is around 1 eV (at room temperature). For instance silicon has band gap energy of 1.12 eV.

In semiconductors not only the electrons in the conduction band can move and carry currents, but also the vacancies they leave to the valence band, called holes. When an electron is excited to the conduction band, a vacant energy state, a hole, is generated to the valence band. Another electron can move into this hole, and further a third electron may move to the vacant state of the previous

electron and so on. This apparent motion of holes in the valence band contributes to the current like the motion of electrons in the conduction band. When an electric field is applied, the holes in the valence band move to opposite direction with respect to the electrons in the conduction band, although the moving charge carriers are actually electrons in both bands. This feature, observed in pure semiconductors, is known as intrinsic conductivity [1], [3].

Then it must be considered how an electron can obtain the required energy to jump to the conduction band. Thermally is obviously one way, but in photovoltaic the energy is received from the photons of solar radiation. To excite an electron for instance in a silicon crystal, a photon with energy of 1.12 eV is required. The energy of a photon is related to its frequency with the following expression [1].

$$E = h\upsilon = hc\lambda \quad \text{.....(2.1)}$$

Where, h is the Planck's constant ($6.626 \cdot 10{-}34$ Js), ν is the photon's frequency (Hz), λ is its wavelength (m) and c is the speed of light ($2.998 \cdot 108$ m/s). The speed of light is related to the frequency and wavelength with the expression $c = \nu\lambda$. [1] Using equation (2.1) it can be calculated that in silicon photons with wavelengths shorter than 1.11 μm are able to excite an electron to the conduction band. Photons with wavelengths longer than 1.11 μm cannot do this, but their energy is wasted as heat. On the other hand, as only the exact amount of 1.12 eV is utilized by the excited electron, photons with wavelengths shorter than the limit have excess energy that also heats the cell. This means that in the case of silicon 20.2% of the sun's energy is wasted due to photons with too long, and 30.2% due to photons with too short wavelengths, giving a theoretical upper limit of 49.6% for the efficiency of a single junction silicon solar cell (from figure 2.2). In real silicon solar cells, however, the highest efficiencies that have been obtained in laboratories are in the order of 25%. The remaining 20% is lost due to various reasons, such as [1]:

- some of the photons are reflected from the surface of the cell and some pass right through the cell
- part of the generated electron-hole pairs are recombined before they contribute to the current
- the cell has some internal resistance.

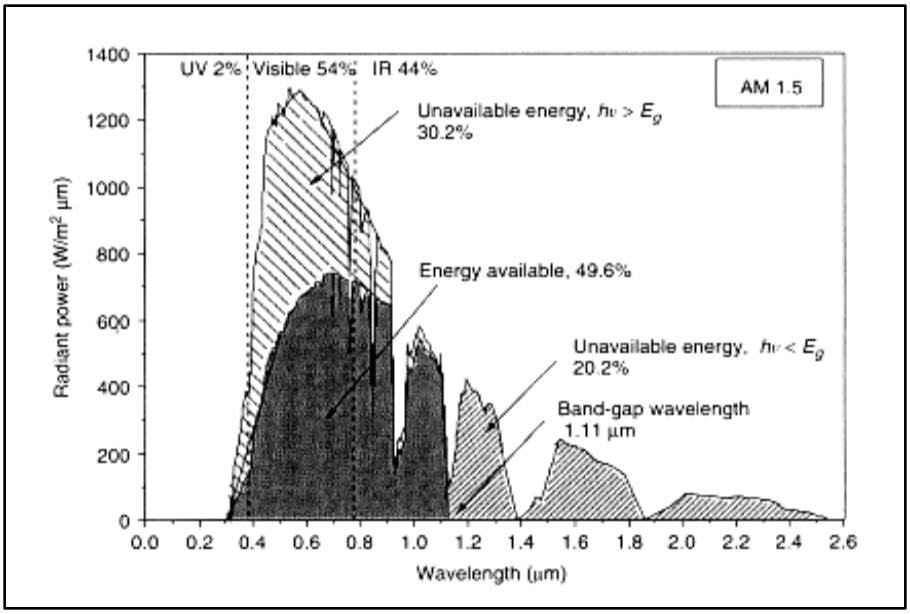

Figure 2.2.The solar spectrum at AM1.5. [1]

In figure 2.2,dark area Indicated are the portion of the sun's energy that can be exploited by a silicon solar cell and the sparse stripes portions of energy wasted for photons with excess energy and for photons with shortage of energy [1].

It is the size of the band gap of the material used that determines the theoretical upper limit for the efficiency of a solar cell. With lower band gap energy, there are more photons with the ability to excite electrons to the conduction band, resulting in a higher current; on the other hand, there are also more photons with excess energy that is wasted as heat. With higher band gap energy in turn, less electrons are excited, but the electrons have more energy and there are also less photons with excess energy to be dissipated. Thus, a smaller band gap yields more current and less voltage, and a higher band gap gives the opposite. The optimum band gap, that results in the highest possible power and efficiency, is estimated to be between 1.2 eV and 1.8 eV [1] – the band gap of silicon is thus slightly too small.

The Silicon properties are given below in table 2.1[4].

Table2.1. Properties of a Silicon Material

Property	**Value**
Atomic Density	5×10^{22} cm^{-3} 5×10^{28} m^{-3}
Atomic Weight	28.09
Density (ρ)	2.328 g cm^{-3} 2328 kg m^{-3}
Energy Band gap (E_G)	1.1242 eV
Intrinsic Carrier Concentration (n_i) at 300K	1×10^{10} cm^{-3} 1×10^{16} m^{-3}
Intrinsic Carrier Concentration (n_i) at 25°C	8.6×10^{9} cm^{-3} 8.6×10^{15} m^{-3}
Lattice Constant	0.543095 nm
Melting Point	1415 °C
Thermal Conductivity	1.5 $Wcm^{-1}K^{-1}$ 150 $Wm^{-1}K^{-1}$
Thermal Expansion Coefficient	2.6×10^{-6} K^{-1}
Effective Density of States in the Conduction Band (N_C)	3×10^{19} cm^{-3} 3×10^{25} m^{-3}
Effective Density of States in the Conduction Band (N_V)	1×10^{19} cm^{-3} 1×10^{25} m^{-3}
Relative Permittivity (ε_r)	11.7
Electron Affinity	4.05 eV
Electron Diffusion Coefficient (D_e)	kT/q μ_e
Hole Diffusion Coefficient (D_h)	kT/q μ_h

2.2.Doping

Semiconductors are very sensitive to impurities. This property can be exploited in changing their conductivity in a more favorable direction by adding suitable impurities, which is called doping. Semiconductors can be doped so that there is excess or shortage of electrons, to make n- or p-type semiconductors, respectively. When p- and n-type material is brought into contact, a p-n junction is formed.

Electrical conduction in intrinsic semiconductors is quite poor at room temperature. Semiconductors are doped to improve their conductivity and to get the required ingredients for the p-n junction:

- p--type semiconductors
- n-type semiconductors

2.2.1. P-type Semiconductor

To produce p-type semiconductor, group III elements are introduced to the semiconductor. Silicon is typically doped with boron, with approximate concentrations of one boron atom per ten million silicon atoms. Again, each boron atom substitutes a silicon atom in the silicon crystal, and is surrounded by four silicon atoms. Boron has three valence electrons that are all bound to the adjacent silicon atoms, but now an extra hole, a vacant energy state, is left next to the boron atom. This hole is easily filled by electrons from nearby atoms, and can therefore be thought as a mobile positive charge. As the hole is filled, the boron atom having a +5e charge in its nucleus is surrounded with all together six electrons – thus a fixed ion with net charge of −e is formed. As boron atoms accept electrons, they are called acceptors. A semiconductor doped with an acceptor is called p-type semiconductor because of its free positive charge carriers [1], [3].

It is important to remember that despite their names, p- and n-type semiconductors are electrically neutral. The names merely refer to the type of majority charge carriers in these materials – electrons in n-type and holes in p-type semiconductors.

2.2.2. N-type Semiconductor

N-type silicon is produced by introducing a small portion of some group V element, typically phosphorus, into the silicon crystal. Typically a ratio of approximately one phosphorus atom per 1000 silicon atoms is used – already this is sufficient to change the conductivity properties of silicon significantly. A phosphorus atom takes place of a silicon atom in the crystal lattice, and out of the five valence electrons of phosphorus, four are tied with covalent bonds to the adjacent silicon atoms. The fifth electron, however, is very loosely bound, and requires very little energy to be excited to the conduction band; at room temperature the fifth electron is most probably found in the conduction band. What the fifth electron then leaves behind is a +15e phosphorus nucleus surrounded by 14 electrons, i.e., an ion with a net charge of +e. This ion is fixed in the crystal lattice – hence there is a fixed net positive charge and a free electron towards each ion. As group V elements donate electrons, they are called donors. This type of semiconductor is called an n-type semiconductor because of the mobile negative charge carriers [1], [3].

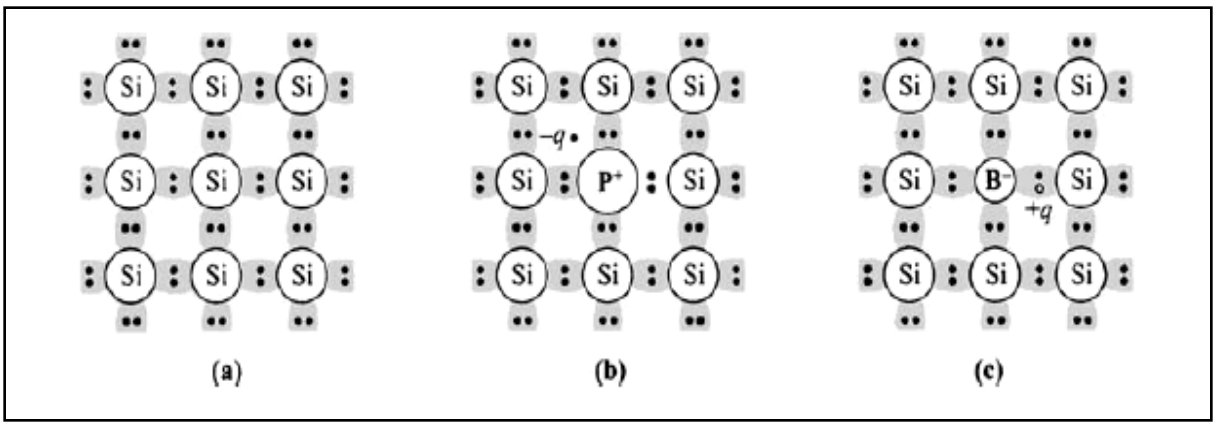

Figure 2.3.Three basic bond pictures of a semiconductor. (a) Intrinsic Si with no impurity.

(b) n-type Si with donor (phosphorus). (c) p-type Si with acceptor (boron).

2.3.Orientation of Monocrystalline Silicon

In single crystalline silicon material the crystal orientation is defined by Miller indices. A particular crystal plane is noted using parenthesis such as (100). Silicon has a cubic symmetrical

cubic structure and so (100), (010) etc are equivalent planes and collectively referred to using braces {100}. Similarly, the crystal directions are defined using square brackets, e.g. [100] and referred collectively using triangular brackets, <100>.

In solar cells the preferred orientation is <100> as this can be easily textured to produce pyramids that reduce the surface reflectivity. However, some crystal growth processes such as dendritic web <111> produce material with other orientations.

To denote the crystal directions, single crystal wafers often have flats to denote the orientation of the wafer and the doping. The most common standard is the SEMI standard:

If the minor flat is 180° from the major flat the wafer is n-type <100>

If the minor flat is 90° to the left or right the wafer is p-type <100>.

If the minor flat is 45° up on the left or right the wafer is n-type <111>

If there are no minor flats the wafer is p-type <111>

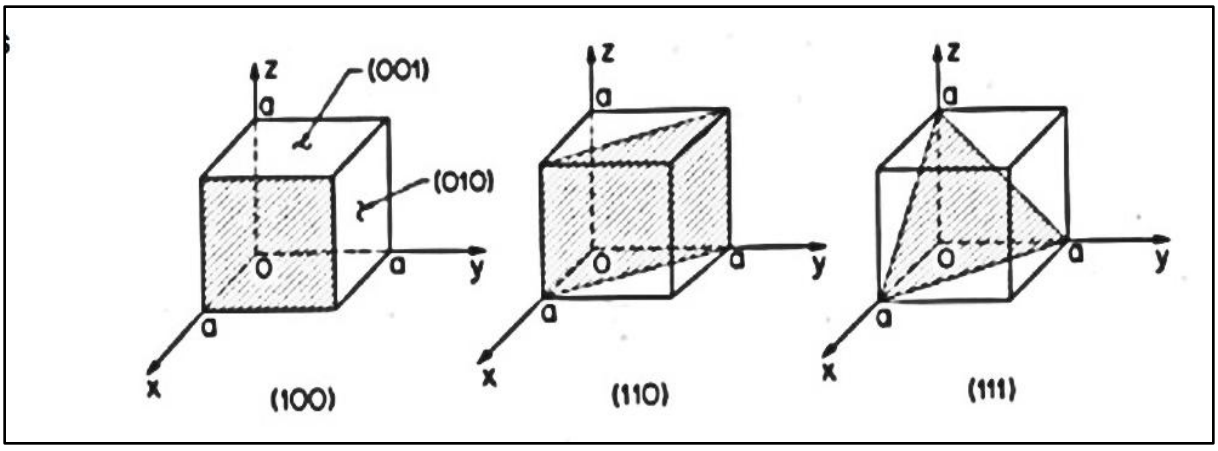

Figure 2.4. Crystal orientation of monocrystalline silicon [4]

2.4.P-N Junction for diode and solar cell

P-n junction diodes form the basis not only of solar cells, but of many other electronic devices such as LEDs, lasers, photodiodes and bipolar junction transistors (BJTs). A p-n junction aggregates the recombination, generation, diffusion and drift effects.

P-n junctions are formed by joining n-type and p-type semiconductor materials, as shown below. Since the n-type region has a high electron concentration and the p-type a high hole concentration, electrons diffuse from the n-type side to the p-type side. Similarly, holes flow by diffusion from the p-type side to the n-type side. If the electrons and holes were not charged, this diffusion process would continue until the concentration of electrons and holes on the two sides were the same, as happens if two gases come into contact with each other. However, in a p-n junction, when the electrons and holes move to the other side of the junction, they leave behind exposed charges on doping atom sites, which are fixed in the crystal lattice and are unable to move. On the n-type side, positive ion cores are exposed. On the p-type side, negative ion cores are exposed. An electric field ε forms between the positive ion cores in the n-type material and negative ion cores in the p-type material. This region is called the "depletion region" since the electric field quickly sweeps free carriers out, hence the region is depleted of free carriers. A built in potential V_{bi} due to ε is formed at the junction.

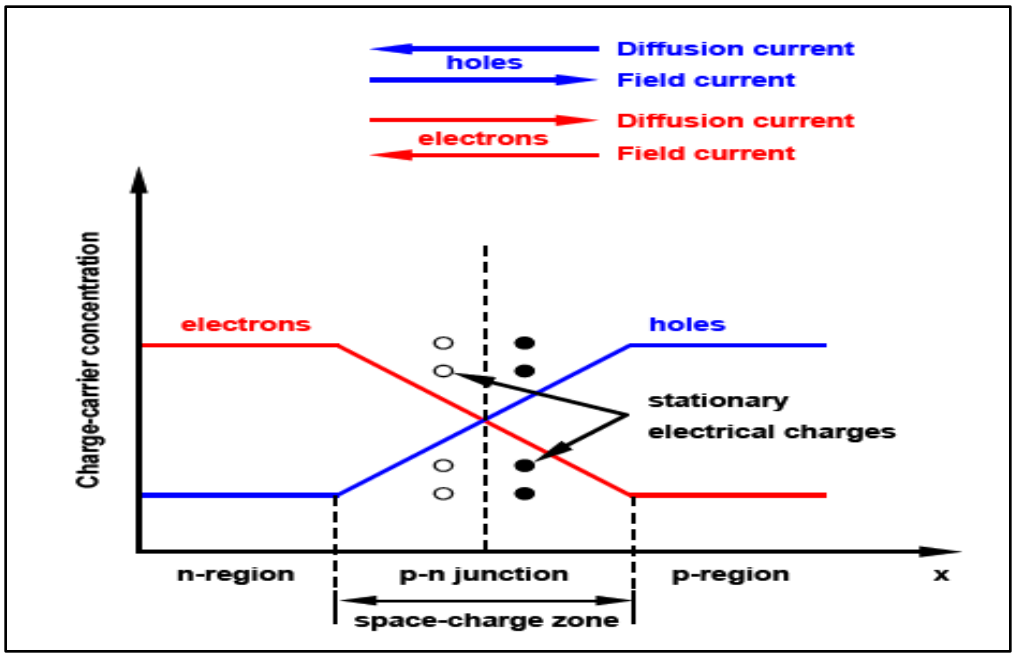

Figure 2.5.Charge carrier distribution at p-n junction and currents through the junction [5]

The diode equation gives an expression for the current through a diode as a function of voltage. The Ideal Diode Law, expressed as:

$I = I_0 \left(e^{\frac{qv}{kT}} - 1 \right)$ [11]

Where, I =the net current flowing through the diode

I_0 = dark saturation current

v=applied voltage across the terminals of the diode

q= absolute value of electron charge

k = Boltzmann's constant

T = absolute temperature (K)

The "dark saturation current" (I_0) is an extremely important parameter which differentiates one diode from another. I_0 is a measure of the recombination in a device. A diode with a larger recombination will have a larger I_0.

For actual diodes, the expression becomes:

$$I = I_0 \left(e^{\frac{qv}{nkT}} - 1 \right) \text{ [6]}$$

Where,

n = Ideality factor, a number between 1-2

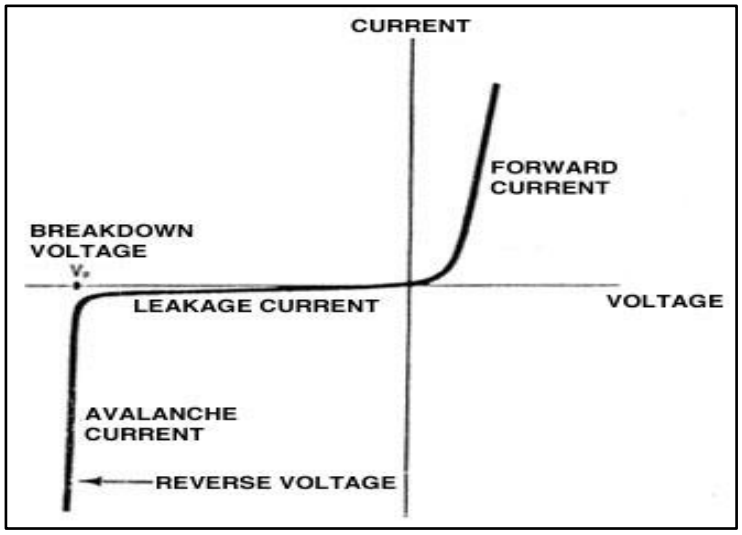

Figure 2.5. I-V Characteristics curve of an ideal p-n junction diode [7]

The collection of light-generated carriers does not by itself give rise to power generation. In order to generate power, a voltage must be generated as well as a current. Voltage is generated in a solar cell by a process known as the photovoltaic effect. The collection of light-generated

carriers by the p-n junction causes a movement of electrons to the n-type side and holes to the p-type side of the junction.

Under short circuit conditions, there is no buildup of charge, as the carriers exit the device as light-generated current. However, if the light-generated carriers are prevented from leaving the solar cell, then the collection of light-generated carriers causes an increase in the number of electrons on the n-type side of the p-n junction and a similar increase in holes in the p-type material. This separation of charge creates an electric field at the junction which is in opposition to that already existing at the junction, thereby reducing the net electric field. Since the electric field represents a barrier to the flow of the forward bias diffusion current, the reduction of the electric field increases the diffusion current. A new equilibrium is reached in which a voltage exists across the p-n junction. The current from the solar cell is the difference between load current and the forward bias current.

Under open circuit conditions, the forward bias of the junction increases to a point where the light-generated current is exactly balanced by the forward bias diffusion current, and the net current is zero. The voltage required to cause these two currents to balance is called the open-circuit voltage.

2.5.Parameters for Efficiency Test

2.5.1. I-V Curve

The I-V curve of a solar cell is the superposition of the I-V curve of the solar cell diode in the dark with the light-generated current. The light has the effect of shifting the I-V curve down into the fourth quadrant where power can be extracted from the diode. Illuminating a cell adds to the normal dark currents in the diode so that the diode law becomes:

$$I = I_0 \left[exp\left(\frac{qv}{nkT}\right) - 1 \right] - I_L \quad [9]$$

Where I_L = light generated current.

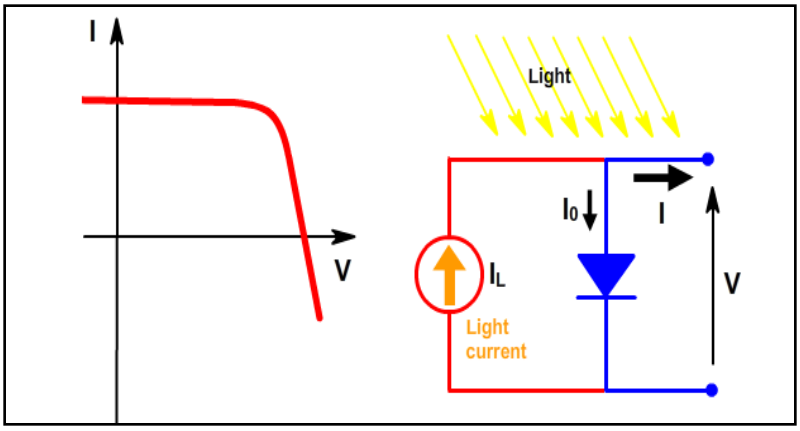

Figure 2.6.The effect of light on the current-voltage Characteristics of a p-n junction [9]

Note: Since the cell is generating power the convention is to invert the current axis

2.5.2. Short-Circuit Current

The short-circuit current is the current through the solar cell when the voltage across the solar cell is zero (i.e., when the solar cell is short circuited). Usually written as I_{SC}, the short-circuit current is shown on the I-V curve in the figure – 2.7. The short-circuit current is due to the generation and collection of light-generated carriers. For an ideal solar cell at most moderate resistive loss mechanisms, the short-circuit current and the light-generated current are identical. Therefore, the short-circuit current is the largest current which may be drawn from the solar cell.

The short-circuit current depends on a number of factors which are described below:

- the area of the solar cell - To remove the dependence of the solar cell area, it is more common to list the short-circuit current density (J_{sc} in mA/cm^2) rather than the short-circuit current [10]
- the number of photons - Isc from a solar cell is directly dependant on the light intensity as discussed in Effect of Light Intensity [10]
- the spectrum of the incident light - For most solar cell measurement, the spectrum is standardized to the AM1.5 spectrum [10]
- the optical properties of the solar cell [10]

- the collection probability - the collection probability of the solar cell which depends chiefly on the surface passivation and the minority carrier lifetime in the base [10]

2.5.3. Open-Circuit Voltage

The open-circuit voltage, V_{OC} is the maximum voltage available from a solar cell, and this occurs at zero current. The open-circuit voltage corresponds to the amount of forward bias on the solar cell due to the bias of the solar cell junction with the light-generated current. The open-circuit voltage is shown on the I-V curve in the figure – 2.7.

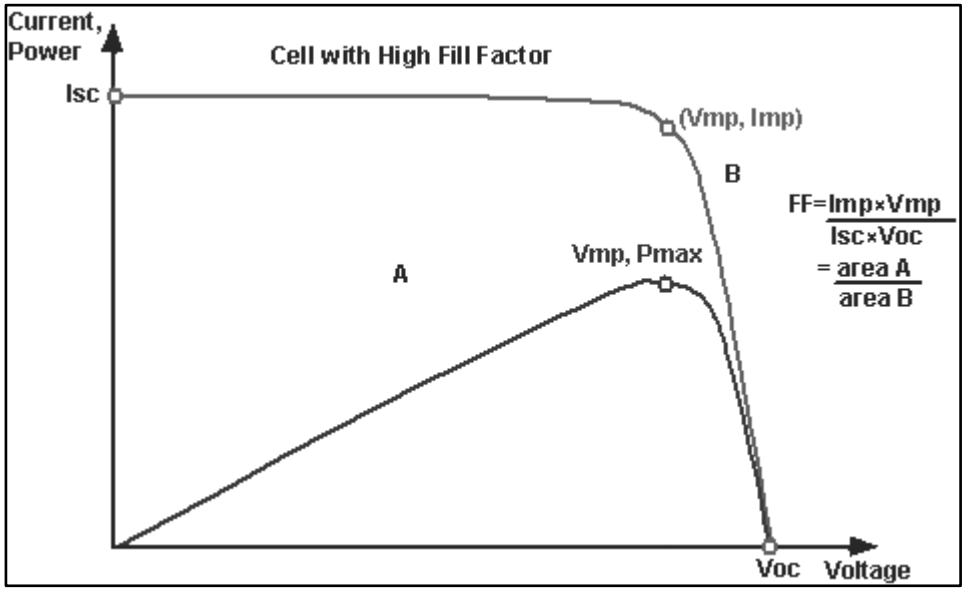

Figure 2.7. I - V curve of a solar cell showing the short-circuit current, open-circuit Voltage, fill factor 'FF', maximum power point (V_{mp}, I_{mp}) [11]

2.5.4. Fill Factor

The short-circuit current and the open-circuit voltage are the maximum current and voltage respectively from a solar cell. However, at both of these operating points, the power from the solar cell is zero. The "fill factor" more commonly known by its abbreviation "FF" is a parameter which, in conjunction with V_{oc} and I_{sc} determines the maximum power from a solar cell. The FF is defined as the ratio of the maximum power from the solar cell to the product of V_{oc} and I_{sc}.

Graphically, the FF is a measure of the "squareness" of the solar cell and is also the area of the largest rectangle which will fit in the I-V curve. The FF is illustrated in the figure-2.10. The FF is most commonly determined from measurement of the IV curve and is defined as the maximum power divided by the product of I_{sc}*V_{oc} [11].

$$FF = \frac{V_{mp} I_{mp}}{V_{oc} I_{sc}} \text{ [11]}$$

2.5.5. Efficiency

The efficiency is the most commonly used parameter to compare the performance of one solar cell to another. Efficiency is defined as the ratio of energy output from the solar cell to input energy from the sun. In addition to reflecting the performance of the solar cell itself, the efficiency depends on the spectrum and intensity of the incident sunlight and the temperature of the solar cell. Therefore, conditions under which efficiency is measured must be carefully controlled in order to compare the performance of one device to another. Terrestrial solar cells are measured under AM1.5 [18] conditions and at a temperature of 25°C [18]. Solar cells intended for space use are measured under AM0 [18] conditions.

The efficiency of a solar cell is determined as the fraction of incident power which is converted to electricity and is defined as:

Efficiency, $n = \frac{P_{max}}{P_{in}}$[12]

Where, $P_{max} = V_{oc} I_{sc} F$ [12]

2.6.Effect of few parameters

2.6.1. Characteristic Resistance

The characteristic resistance of a solar cell is the output resistance of the solar cell at its maximum power point. If the resistance of the load is equal to the characteristic resistance of the solar cell, then the maximum power is transferred to the load and the solar cell operates at its

maximum power point. It is a useful parameter in solar cell analysis, particularly when examining the impact of parasitic loss mechanisms. The characteristic resistance is shown in the figure 2.8.

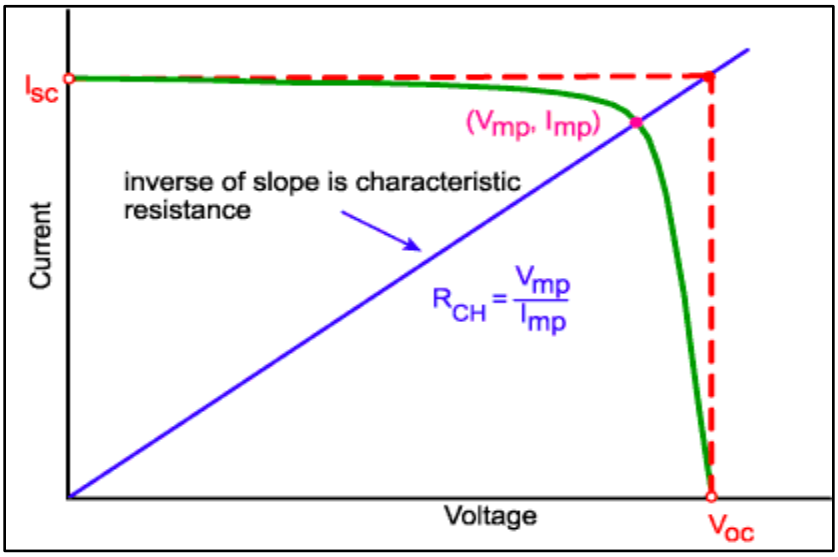

Figure 2.8. The characteristic resistance of a solar cell [13]

The characteristic resistance of a solar cell is the inverse of the slope of the line, shown in the figure above, can be given as:

$$R_{CH} = \frac{V_{MP}}{I_{MP}} = \frac{V_{oc}}{I_{sc}} \qquad [13]$$

The equation for the characteristic resistance is:

$$I = \frac{1}{R_{CH}} V \qquad [19]$$

Substituting the point I_{sc} and V_{oc} in the equations gives:

$$I_{SC} = \frac{1}{R_{CH}} V_{oc} \qquad [13]$$

2.6.2. Effect of Parasitic Resistances

Resistive effects in solar cells reduce the efficiency of the solar cell by dissipating power in the resistances. The most common parasitic resistances are series resistance and shunt resistance. The inclusion of the series and shunt resistance on the solar cell model is shown in the figure 2.9.

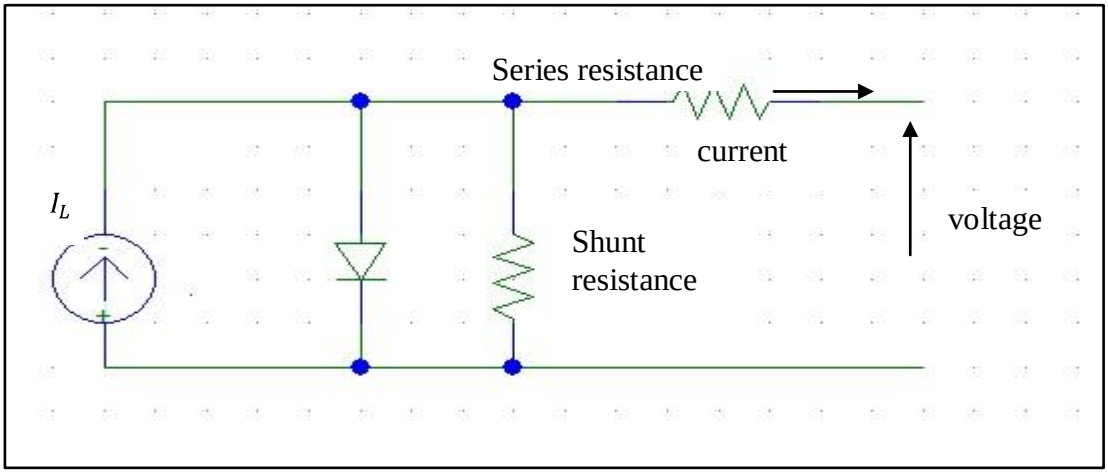

Figure 2.9. Parasitic resistances in a solar cell circuit

In most cases and for typical values of shunt and series resistance, the key impact of parasitic resistance is to reduce the fill factor. Both the magnitude and impact of series and shunt resistance depend on the geometry of the solar cell, at the operating point of the solar cell. Since the value of resistance will depend on the area of the solar cell, when comparing the series resistance of solar cells which may have different areas, a common unit for resistance is in Ωcm^2 [20]. This area-normalized resistance results from replacing current with current density in Ohm's law as shown below:

$$R'(\Omega cm^2) = \frac{V}{J} \qquad [14]$$

2.6.2.1. Series Resistance

Series resistance in a solar cell is due to three causes. Firstly, the movement of the current through the emitter and base of the solar cell. Secondly, the contact resistance between the metal contact and the silicon. Finally, the resistance of the top and rear metal contacts. The main impact of series resistance is to reduce the fill factor, although excessively high values may also

reduce the short-circuit current. The effect of the series resistance on the IV curve is shown in figure – 2.13. Series resistance does not affect the solar cell at open-circuit voltage since the overall current flow through the solar cell, and therefore through the series resistance is zero.

However, near the open-circuit voltage, the I-V curve is strongly affected by the series resistance. A straight-forward method of estimating the series resistance from a solar cell is to find the slope of the I-V curve at the open-circuit voltage point.

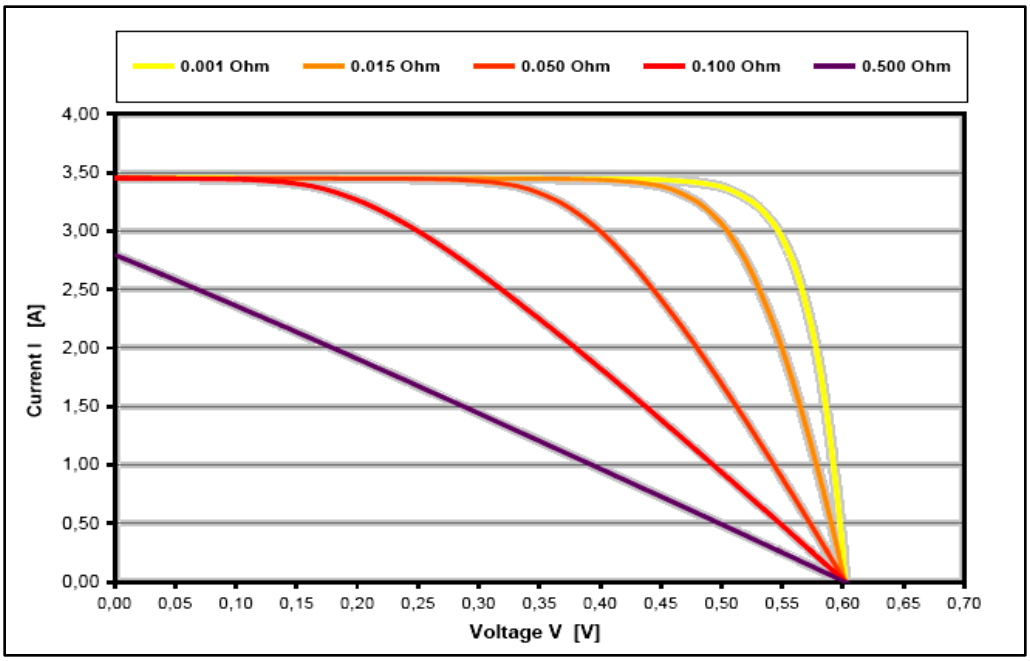

Figure 2.10. I-V curve for different series resistances [14]

2.6.2.2. Shunt Resistance

Significant power losses caused by the presence of a shunt resistance are typically due to manufacturing defects, rather than poor solar cell design. Low shunt resistance causes power losses in solar cells by providing an alternate current path for the light-generated current. Such a diversion reduces the amount of current flowing through the solar cell junction and reduces the voltage from the solar cell. The effect of a shunt resistance is particularly severe at low light levels, since there will be less light-generated current. The loss of this current to the shunt

therefore has a larger impact. In addition, at lower voltages where the effective resistance of the solar cell is high, the impact of a resistance in parallel is large.

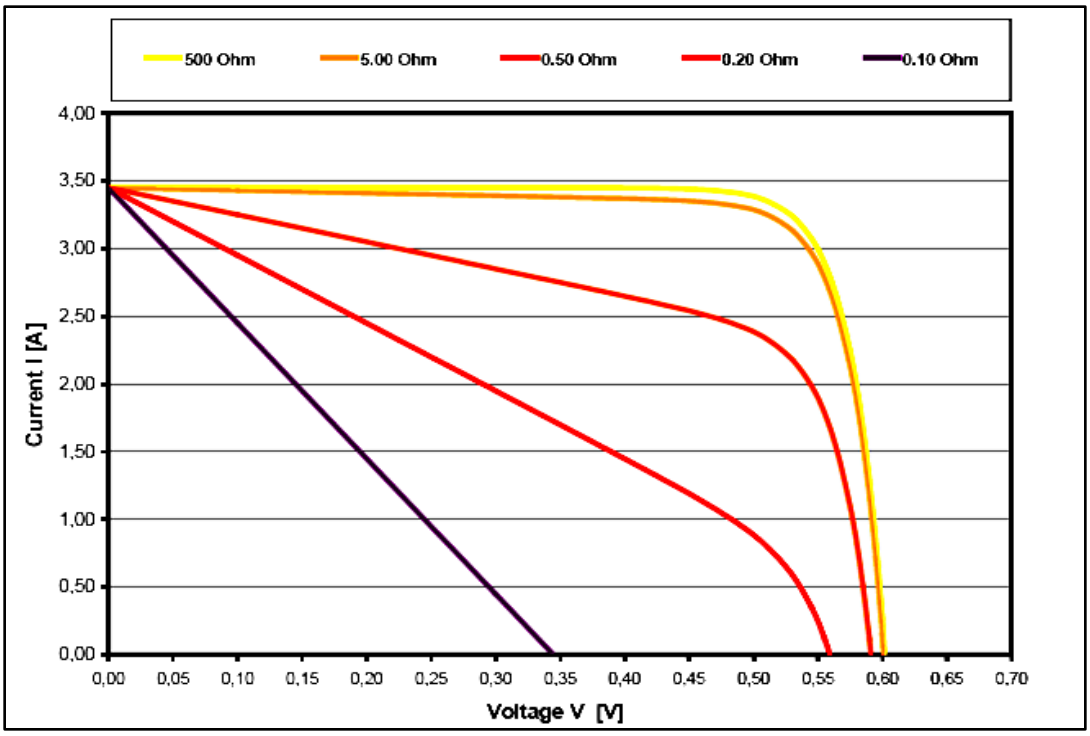

Figure 2.11. I-V curve for different parallel resistances [14]

2.7.Effect of Temperature

Like all other semiconductor devices, solar cells are sensitive to temperature. Increases in temperature reduce the band gap of a semiconductor, thereby effecting most of the semiconductor material parameters. The decrease in the band gap of a semiconductor with increasing temperature can be viewed as increasing the energy of the electrons in the material. Lower energy is therefore needed to break the bond. In the bond model of a semiconductor band gap, reduction in the bond energy also reduces the band gap. Therefore increasing the temperature reduces the band gap.

In a solar cell, the parameter most affected by an increase in temperature is the open-circuit voltage. The impact of increasing temperature is shown in the figure – 2.12.

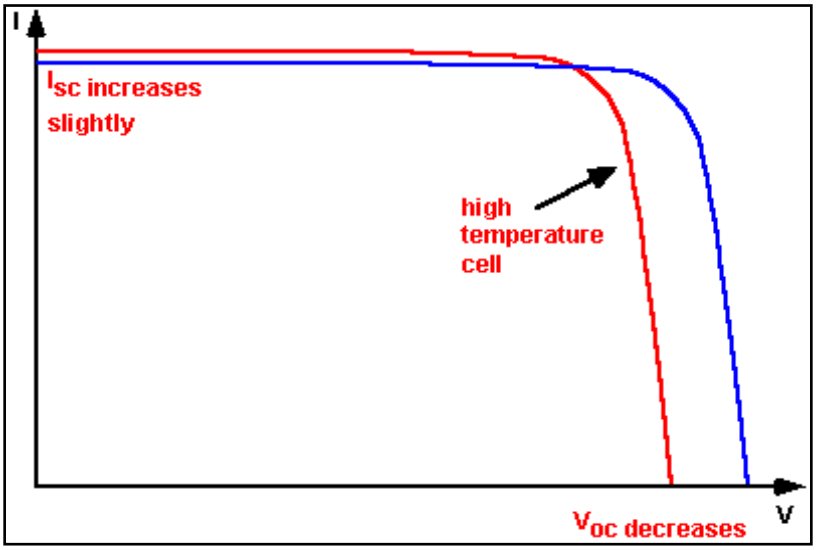

Figure 2.12. Effect of temperature on the IV characteristics of a solar cell [15]

2.8.Effect of Light Intensity

Changing the light intensity incident on a solar cell changes all solar cell parameters, including the short-circuit current, the open-circuit voltage, the FF, the efficiency and the impact of series and shunt resistances. The light intensity on a solar cell is called the number of suns, where 1 sun corresponds to standard illumination at AM1.5, or 1 kW/m^2 [16]. For example a system with 10 kW/m^2[16] incident on the solar cell would be operating at 10 suns, or at 10X [16]. A PV module designed to operate under 1 sun conditions is called a "flat plate" module while those using concentrated sunlight are called concentrators.

Reference

[1] *G. M. Masters. Renewable and Efficient Electric Power Systems. JohnWiley & Sons, 2004.*

[2] Elements Database. Periodic Table of Elements. Retrieved August, 2008 ,
Available: http://www.elementsdatabase.com/.

[3] H. D. Young and R. A. Freedman. University Physics with Modern Physics. Pearson Addison Wesley, San Fransisco, CA, USA, 11th edition,2004.

[4] www.pveducation.org

[5] www.re.e-technik.uni-kassel.de/photos/.../29-SKRIPT_Photovoltaic.pdf

[6]. http://PVeducation.org/PVcdrom/pn-junction/diode-equation

[7]http://ingles-escrito-es.wikispaces.com/The+diode

[8] www.pveducation.org,n.d.

[9]http://PVeducation.org/PVcdrom/solar-cell-operation/iv-curve

[10] http://PVeducation.org/PVcdrom/solar-cell-operation/short-circuit-current

[11] http://PVeducation.org/PVcdrom/solar-cell-operation/fill-factor

[12] http://PVeducation.org/PVcdrom/solar-cell-operation/efficiency

[13] http://PVeducation.org/PVcdrom/solar-cell-operation/charecteristic-resistance

[14]http://PVeducation.org/PVcdrom/solar-cell-operation/effect-of-parasitic-resistances

[15] http://PVeducation.org/PVcdrom/solar-cell-operation/effect-of-temperature

[16] http://PVeducation.org/PVcdrom/solar-cell-operation/effect-of-light-intensity

Chapter 3

Monocrystalline Solar Cell Fabrication

3.1.Introduction

The fabrication of our silicon solar cell starts with a 200μm thick, (100) oriented Czochralski Si (or Cz-Si) wafer. The majority of silicon solar cell production is currently based upon a very standardized process that is intended to make a p-n-electrical junction on the entire front surface of the wafer and a full-area aluminum-based metallization on the back [1]. The wafers generally have micrometer sized surface damages that need to be removed. After the damage removal, the wafer surface shows high optical reflectivity, for which an anti-reflection coating (ARC) is necessary. Furthermore, the top surface was textured by chemical etching before an ARC was deposited.

For a p-type crystalline silicon (c-Si) substrate, an n-type top layer while for an n-type c-Si substrate a p-type top layer acts as emitter. A thermal diffusion is commonly used for emitter diffusion [2]. After the emitter diffusion, the edge isolation was carried out, as otherwise the top and the bottom surfaces of the wafers remain electrically shorted. A suitable thin dielectric coating at the front and back of the wafers were given to passivate surface defects. As the wafer becomes covered with a dielectric layer, an electrical connection to the cell becomes necessary. Ag and Al metal electrodes were formed by using screen printing of Al pastes and co-firing at a suitable temperature.

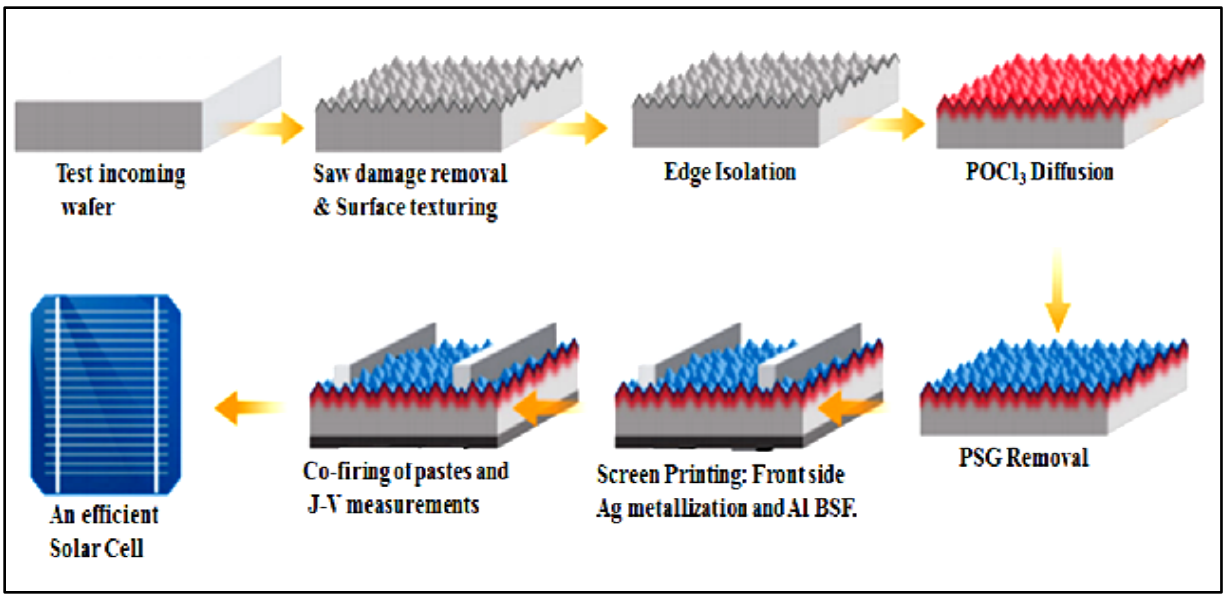

Figure 3.1. Steps of solar cell fabrication process [3]

3.2.Fabrication Steps

3.2.1. Test Incoming Wafer

Wafers are typically received from multiple supply sources, and because they can be damaged during sawing and shipping, all incoming wafers should be tested to ensure that they would provide a foundation for acceptable cell efficiencies [4].

3.2.2. Saw Damage Removal

In a solar cell, contribution from both the surface and volume of the wafer are needed. Therefore, cleaning of Si wafers is essential in order to remove the organic and inorganic contaminants from the c-Si wafer surfaces.

Wet-chemical treatments are an important step in the silicon solar cells fabrication. Process carried out in wet-chemical bench is called Etching. We have used some standard process called Radio Corporation America (RCA) cleaning.

Process 1

The surface damages to the wafers were removed by using RCA cleaning process consists of two steps normally referred to as standard cleaning 1 (SC1) and standard cleaning 2 (SC2).
The SC1 step consisting of a NH4OH/H2O2/H2O mixture, aims at organic particle removal.
For SC2 step, HCl/H2O2/H2O mixture is used to remove metal or inorganic contaminants.
Figure 1 show the DI water rinsing as first step in cleaning process. Figure 2 show the wafers dip into the nitric acid solution and start the RCA clean process.

Figure 3.2.RCA cleaning process: DI water dip(left),cleaning process: Nitric Acid solution(Right)

Process 2

The surface damages to the wafers were removed through isotropic etching with a concentrated solution of NaOH in de-ionized water (DI-W). DI-W helps the NaOH to break in Na+ and OH^- ions in the solution. A 10% NaOH solution, at 70°C temperature for about 10 minutes of etching removes the organic contaminants.

3.2.3. Hydrophobic Process

Saw damage removal step etches out about 5 micro meter Si from wafer surface. After that the wafers were rinsed in DI-W for 1 min, HF (2%) for 1 min, DI-W for 1 min.After that the wafers are dried using compressed air or nitrogen blow so that they are prepared for the next step.

Figure 3.3 shows the Scanning Electron Microscopic (SEM) images of raw wafer and saw damage removed wafer [5]

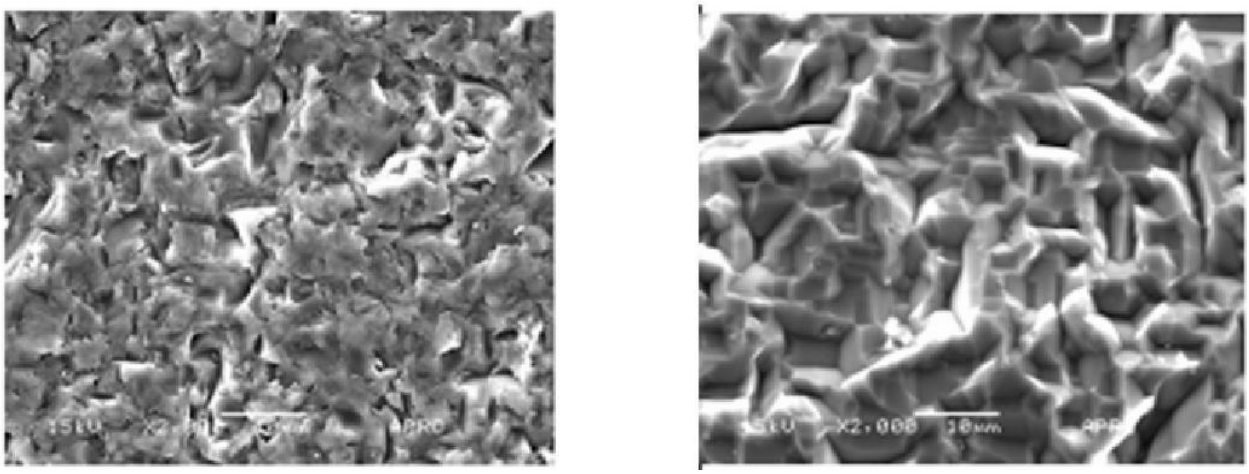

(a). Raw wafer (b). Saw damage removed surface

Figure 3.3. Comparison of SEM image of the (a) raw wafer and (b) saw damage removed wafer [5]

3.2.4. Surface Texturing Process

Surface texturing is used to enhance the amount of light absorbed into devices by reducing reflection losses. In addition, surface texturing scatters light inside the semiconductor in order to trap it inside the wafer, and therefore increases the short circuit as well as the efficiency of the solar cells. KOH/IPA texturing process is used to create random pyramid features on wafer surface to reduce reflection and enhance light absorption.

For this process, a wet bench chemical treatment was utilized to etch away between 5 and 15μm of silicon wafer from the top surface. The characteristics of the etching depend upon, time of etching, etching rate, temperature, components of the solution and its concentration. IPA enhances surface diffusion, so a rapid etching can take place in presence of IPA in the solution [18]. With the alkali metal only being a spectator ion, the etching reaction proceeds as follows [19]:

$$Si + 2KOH + H_2O\ K_2\ SiO_3 + 2H_2$$

The potassium silicate (K2SiO3) is soluble in water and thus silicon surface remains devoid of any deposition. For texturing process, we prepared a solution using the ratio of, KOH: IPA: H2O = 1 gram: 5 ml: 125 ml.

Initially DI water was transferred to a clean beaker and then KOH pellet was added to the beaker. The solution was then heated and when it reached at 70°C temperature, we dipped the silicon wafer and added IPA into that solution. After 10 minutes the wafers ware removed from the beaker and rinsed with DI-water then the hydrophobic process was repeated and finally the wafers ware dried using the compressed air.

Figure 3.4. After Clean Wafers in Texturing process [6]

Figure 3.5. Compress air gun for wafer drying [6]

3.2.4.1. Result

SEM image/ structural characterization of textured sample:

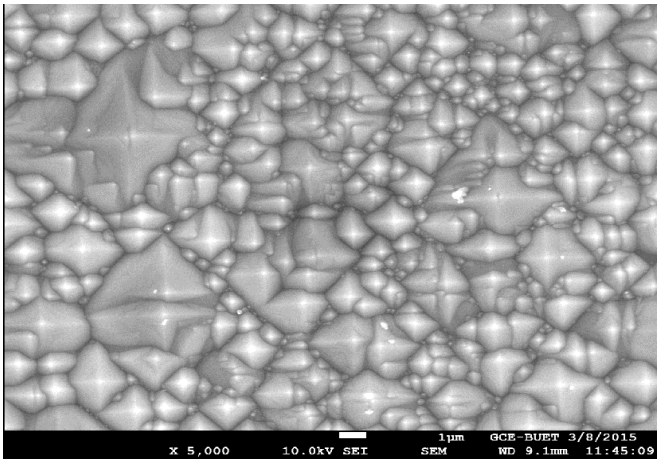

Figure 3.6. SEM of the p-type textured silicon wafer [3]

In this anisotropic texturing process both faces of the wafer covers by micrometer sized four sided pyramids. Pyramids are of [111] planes. That means [111] planes formed on [100] oriented surface.

3.2.5. Phosphorus Diffusion Process

For boron doped p-type silicon substrate, an n-type top layer acts as emitter. A thermal diffusion is commonly used for emitter diffusion [7] [8]. Phosphorus (P) diffusion is currently the primary method for emitter fabrication in silicon (Si) solar cell processing [9] [10]. Along with nitrogen (N2) and oxygen (O2) gases, phosphorus oxy-chloride (POCl3), a liquid source of phosphorus, is also widely used in the standard diffusion process of solar cells [11], [12].The diffusion depends on various factors, of which temperature and gaseous environment is most important [13]. In oxygen environment and at high temperature, phosphorus diffusion leads to formation of n+ type emitter at the top surface of the wafer.

The diffusion was carried out in two stages, pre-deposition and drive-in [14], [15]. The formation of phosphorous-rich oxide films, phosphor silicate glass (PSG), on the silicon substrate carry out at pre-deposition stage and in drive-in stage, the phosphorous-rich oxide film acts as an infinite source for phosphorous diffusion into the Si substrate. The phosphorus atoms formed at the PSG-Si interface penetrate through the silicon wafer [10] and can besimplified with the following reaction equations:

pre-deposition:

$POCl_3$ (liquid) + N_2 (bubble) → POCl3 (vapor)
$POCl_3 + 3O_2 \rightarrow 2\ P_2O_5 + 6Cl2$

drive-in:
$2\ P_2O_5 + 5Si \rightarrow 4P + SiO_2$
P + 3Si → n-type doped Si

Diffusion steps

i. At first the wafers are put inside the diffusion chamber with an initial temperature is 600°C.
ii. Then turn ON N_2 gas and wait for 10 minutes.
iii. Then increase the temperature to 875°C keeping N_2gas turn ON.
iv. When temperature reaches at 875°C turn OFF N_2 gas, turn ON 0_2gas and $POC1_3$ simultaneously.
v. This process continues for 10 minutes.
vi. Then turn OFF 0_2 gas and $POC1_3$ simultaneously and turn ON N2.
vii. After that wait for 10 minutes.
viii. Then turn OFF N_2 and turn ON 0_2 and wait for 10 minutes.
ix. Again turn OFF 0_2 and Turn ON N_2gas and wait for 10 minutes.
x. Then reduce the temperature to 600°c keeping N_2 turn ON.
xi. At 600°c, turn OFF N_2 gas.

Figure 3.7. The phosphorus doped silicon wafer [3]

In presence of oxygen, phosphor silicate glass (PSG) is formed at the 850°C temperature. Phosphor silicate glass or PSG is phosphorus doped silicon dioxide, a hard material layer formed at the top surface of Si wafer in the pre-deposition stage of diffusion process [16]. In the drive-in stage, a deeper junction was formed as phosphorus atoms from the PSG layer diffuse deeper, thus thicker emitter and a lower surface concentration of dopant was achieved. But a thin PSG layer was still present on top of the wafer after drive-in stage of diffusion. Due to this thin phosphor silicate glass (PSG) layer the top wafer surface becomes glassy and degrade blue response of solar cells. To remove the PSG layer we prepared a 10% hydrofluoric acid (HF) solution and then dipped the silicon wafer for one minute after that the wafer were rinsed with DI-water.

3.2.6 Edge Isolation

A critical step in solar cell fabrication is electrical isolation of n and p type regions. Edge isolation is done to separate front side and back side. By using an acid barrier paste with the help of screen printing to isolate the edge. After the screen printing is done the wafers are dried for 10 minutes in a preheated oven at 200 °C.

Figure 3.8(a) shows a screen printer used and (b) screen printing dice

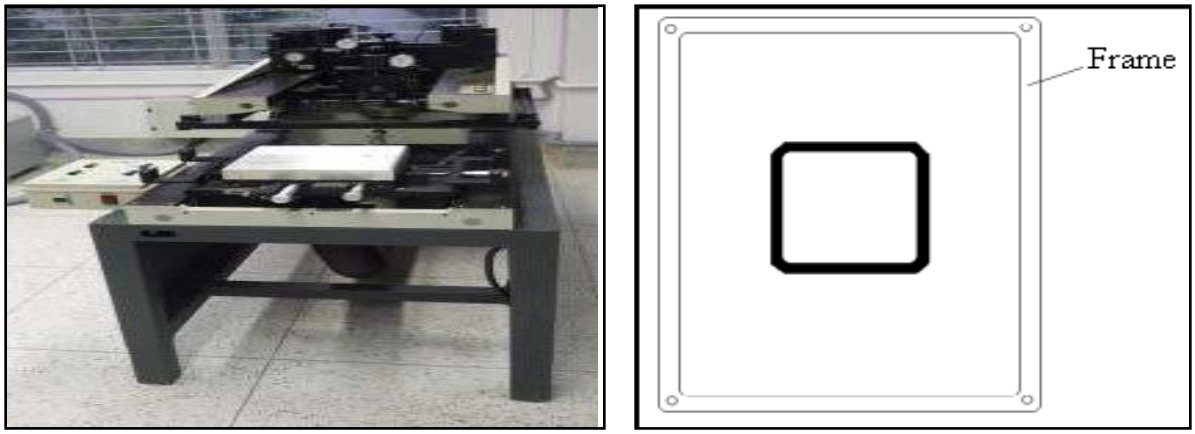

Figure 3.8. (a) Screen printer (b) screen printing frame [20]

3.2.7 Back and front contact /surface metallization

Screen printing process is most commonly used to form metal contacts on back and front surfaces of solar cells. It is cost effective, robust, simple, inexpensive, and fast method of metallization of the solar cells [17][18]. The screen printing of Ag and Al pastes for the formation of the front and rear electrical contacts has been in use by the silicon industrial community since the 1970s [19]. At the front surface the metallization creates electrical connection to thin n+ layer whereas at the back surface it provides an electrical connection and at the same time it creates a p+ layer. Chemicals are Ferro FX53-038, aluminum type for rear surface and Ferro CN33-462, silver type for front surface. The screen is made up of an interwoven mesh kept at a high tension, with an organic emulsion layer defining the printing pattern. Figure 3.10 shows a microscopic image of the screen and the screen mask. An H-pattern screen that was mounted in an aluminum frame was then overlain on the front side of the cell and the metallization paste was squeegeed over the wafer surface with a screen printer.

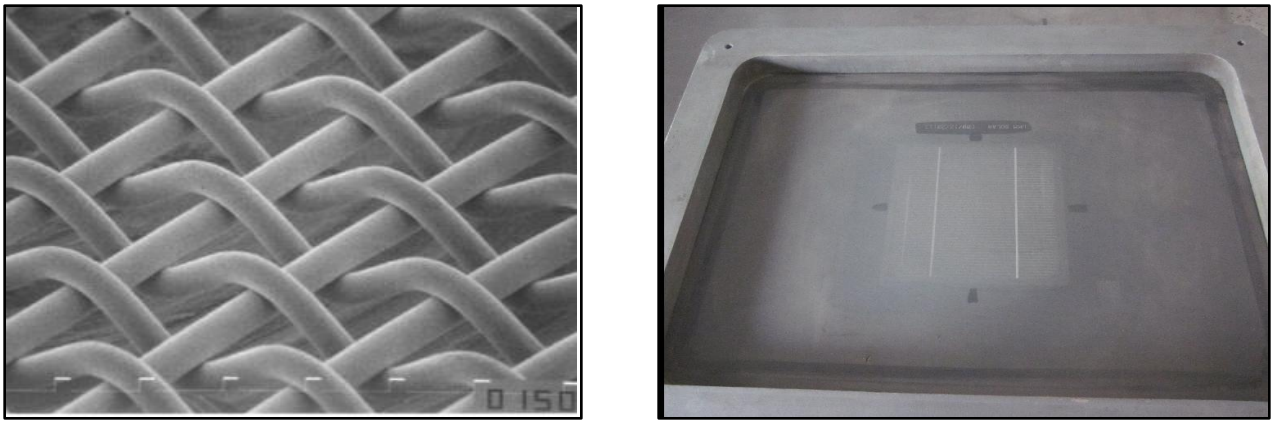

Figure 3.10. a) Microscopic image of the screen b) Image of front side printing mask [3]

After every steps of screen printing, the silicon wafers are required to go through drying at relatively low temperature for certain period in a preheated oven at 120°C for 10 minutes so that the paste gets attached well to the wafer surface.

3.2.8 Co-firing by Rapid Thermal Annealing

In order to establish an ohmic contact (low resistive contacts), contact firing is recommended in silicon solar cell processing. In this case, a belt conveyer system integrated RTA processing unit is used for a continuous processing of contact firing. A convey or belt furnace capable of reaching 1000 °C temperature. RTA of screen printed cells is done at a temperature of 500, 600 and 800 °C respectively. The wafers are passed through a moving belt which goes inside the RTA machine. Figure 3.11 shows the contact firing process of screen printed Si solar cell.

Figure 3.11. Contact firing at RTC furnace [3]

References

[1] J. F. Nijs, J. Szlufcik, J. Poortmans, S. Sivoththaman and R. P. Mertens, "Advanced Manufacturing Concepts for Crystalline Silicon Solar Cells," IEEE Transaction on Electron Devices, vol. 46, pp. 948-969. 1999.

[2] Mrwa, A., Ebest, G., Rennau, M., & Beyer, A. (2000). Comparison of Different Emitter Diffusion Methods for MINP Solar Cells: Thermal Diffusion and RTP. Solar Energy Materials & Solar Cells, 61(2), 127-134.

[3] Md. Abdur Rafiq Akand, Mohammad Khairul Basher, Md. Asrafusjaman, Nusrat Chowdhury, Atia Abedin, and Mahbubul Hoq," Study and Fabrication of Crystalline Silicon Solar Cell in Bangladesh; Using Thermal Diffusion Technique", International Journal of Innovation and Scientific Research
ISSN 2351-8014 Vol. 18 No. 2 Oct. 2015, pp. 417-426

[4] A. Goodrich, P. Hacke, Q. Wang, B. Sopori, R. Margolis, T. L. James and M. A. Woodhouse, "Wafer-based
Monocrystalline Silicon Photovoltaics Road Map: Utilizing Known Technology Improvement Opportunities for Further Reductions Inmanufacturing Costs," Solar Energy Materials & Solar Cells, vol. 114, pp. 110–135, 2013.

[5] E. Vazsonyi, C. Ducso and A. Pekker, "Characterization of the Anisotropic Etching of Silicon in Two-Component Alkaline
Solution," Journal of Micromechanics and Microengineering, vol. 17, pp. 1916-1922, 2007.

[6] Chemical wet bench and furnaces, K. Jayshree, Facilities at Centre of Excellence in Nanoelecctronics
(2009).

[7] A. Mrwa, G. Ebest, M. Rennau and A. Beyer, "Comparison of Different Emitter Diffusion Methods for MINP Solar Cells: Thermal Diffusion and RTP," Solar Energy Materials & Solar Cells, vol. 61no. 2,pp. 127-134, 2000.

[8] M. M. Hilali, A. Rohatgi and S. Asher, "Development of Screen-Printed Silicon Solar Cells with High Fill Factors on 100 Ohm/sq. Emitters," IEEE Transaction on Electron Devices, vol. 51, pp. 948-955, 2004.

[9]A. Bentzen, J.S. Christensen, B.G. Svensson and A. Holt, "Understanding Phosphorus Emitter Diffusion in Silicon Solar Cell Processing," Proceedings of the 21th European Photovoltaic Solar Energy Conference, Dresden, Germany, pp. 1388-1391, 2006.

[10] J. Bultman, I. Cesar, B. Geerligs, Y. Komatsu and W. Sinke, "Methods of Emitter Formation for Crystalline Silicon Solar Cells," Photvoltaics International, vol. 8, pp. 69–80, 2010.

[11] H. Nakaya, M. Nishida, Y. Takeda, S. Moriuchi, T. Tonegawa, T. Machida and T. Nunoi, "Poly Crystalline Silicon Solar Cells with V-grooved Surface," Solar Energy Materials and Solar Cells, vol. 34, pp. 219-225, 1994.

[12] A. Rohatgi, Z. Chen, P. Sana, J. Crotty and J. Salami, "High Efficiency Multi-crystalline Silicon Solar Cells," Solar Energy Materials and Solar Cells, vol. 34, pp. 227-236, 1994.

[13] G. Masetti, S. Solmi and G. Soncini, "On Phosphorus Diffusion in Silicon under Oxidizing Atmospheres," Solid-State Electronics, vol. 16, pp. 419-421, 1973.

[14] D. Kumar, S. Saravanan and P. Suratkar, "Effect of Oxygen Ambient During Phosphorous Diffusion on Silicon Solar Cell," Journal of Renewable and Sustainable Energy, vol. 4, pp. 033105-033113, 2012.

[15] M. Popadic, L. K. Nanver and T. L. M. Scholtes, "Ultra-Shallow Dopant Diffu- sion from Pre-Deposited RPCVD Monolayers of Arsenic and Phosphorus," 15th Inter- national Conference on Advanced Thermal Processing of Semiconductors, pp. 95-100, 2007.

[16] Ilgu Yun, Photodiodes from Fundamentals to Applications", InTech pvt. Limited, ISBN 978-953-51-0895-5, 2012.

[17] T. Kwon, S. Kim, D. Kyung, W. Jung, S. Kim, Y. Lee, Y. Kim, K. Jang, S. Jung, M. Shin and J. Yi, "The Effect of Firing Temperature Profiles for the High Efficiency of Crystalline Si Solar Cells" Solar Energy Materials & Solar Cells, vol. 94, pp. 823-829, 2010.

[18] J. H. Kwon, S. H. Lee, B. K Ju, "Screen-Printed Multi Crystalline Silicon Solar Cells with Porous Silicon Antireflective Layer Formed by Electrochemical Etching," Journal of Applied Physics, vol. 101, pp. 104515-104519, 2007.

[19] E.L. Ralph, "Recent Advancements in Low Cost Solar Cell Processing," Proceedings of the IEEE PVSC, pp. 315-316, 1975.

[20] M. K. Basher, K. M. Shorowordi, "Fabrication of Monocrystalline Silicon Solar Cell using Phosphorous Diffusion Technique", International Journal of Scientific and Research Publications, Volume 5, Issue 3, March 2015 , ISSN 2250-3153

Chapter 4

Monocrystalline Solar Cell Characterization

4.1.Characterization processes

During cell fabrication process there are two processes of characterization of textured surface of Si wafer. One is surface reflection and response (SRR) and another is scanning electron microscope (SEM). Other characterization tests are carried out, after completing the fabrication of a solar cell. These tests show the efficiency of solar cell. The major characterization equipment are LIV tester with which it was possible to evaluate the performance of the cell and mainly to calculate the efficiency of the solar cell, SPV method which relies on analyzing illumination induced changes in the surface voltage and four point probe for measuring sheet and bulk resistance of the cell.

4.2.Surface Reflection and Response (SRR) Method

Surface spectral reflection is determined by measuring the light reflected from the surface of a Si wafer or solar cell as a function of wavelength. Spectral response is determined by measuring the photo-generated I-V response of the solar cell as a function of wavelength. By a careful correlation of spectral reflection, and spectral response, solar cell internal quantum efficiency can be determined.

A simple, computer-controlled, normal incidence measurement system was designed for SRR measurements of Si wafers and solar cells. Measurement system is based on a mini monochromator driven with a stepper motor to vary wavelengths in ~ 500-1200-nm spectral range. Incident light is obliquely incident on the surface of device under test. The resulting signal is connected to a Stanford Research 510 lock-in amplifier. This system can be modified to measure spectral response as a function of wavelength as well as a function of flux density at fixed wavelength. A LabVIEW interface is used for system control and data acquisition.

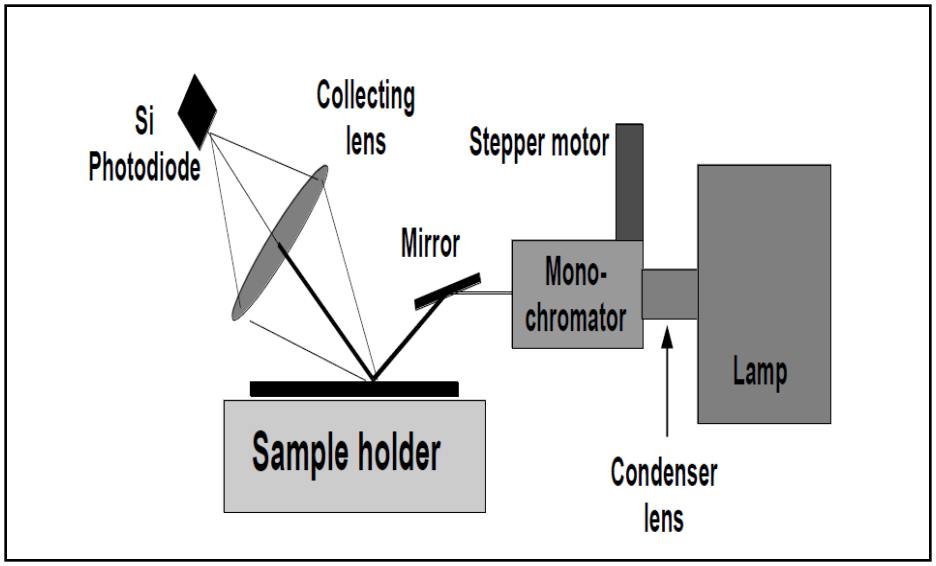

Figure 4.1. Schematic diagram of the surface reflection and measurement system [1]

During normal operation, light from the exit slit of the monochromator is guided to the wafer at near normal incidence. Stepper motor is used to vary monochromator output wavelength. A light chopper is placed at the exit slit of the monochromator to provide reference signal to the lock-in to ensure all the stray light is rejected by the system and enhance system sensitivity from nano-volt to mV range. Surface reflection as a function of wavelength is determined by measuring photo detector response through lock-in amplifier. In order to determine spectral response, completed solar cell with top and bottom contacts is placed on vacuum chuck. Vacuum pump is turned on to ensure low resistivity contact between wafer backside and the vacuum chuck. Current-voltage probes make contact with the front surface (Fig. 4.2) and the back contact is through the Au-coated wafer vacuum chuck. The lock-in output and stepper motor are controlled by a PC using a LabVIEW interface. The system wavelength range is from ~ 500-1000-nm. All data is written to a file in text form for subsequent plotting and processing.

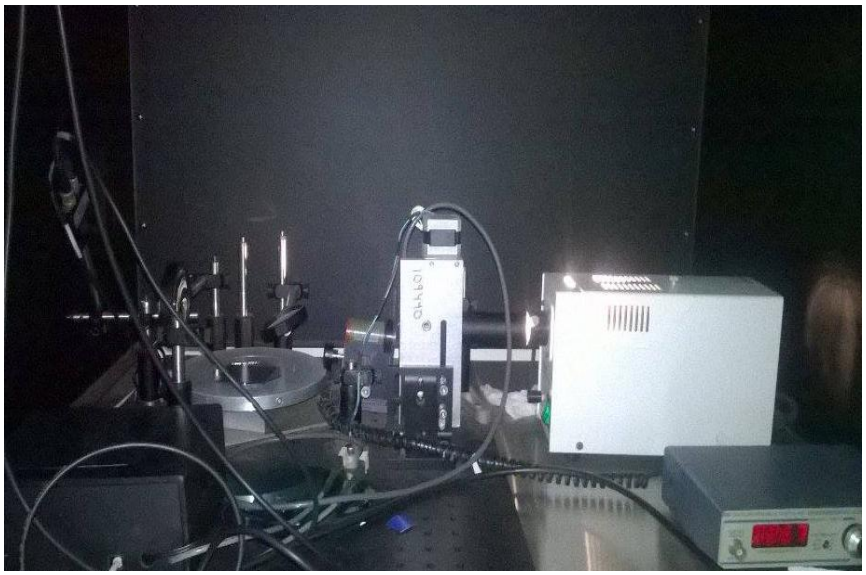

Figure 4.2.Picture of surface reflection

4.3.Scanning Electron Microscope Analysis

The use of the texturization processes to enhance the solar cell efficiency, increasing the light absorption and therefore the short circuit current of the solar cell, must be controlled due to the introduction of new problems in the metallic contact emplacement, poor quality contacts and hot spots. SEM is an interesting tool to control the pyramids size and the formation mechanism involved in the texturization processes. As it has been mentioned in this work, there is a correlation between the pyramids size and the macroscopic parameters as the short-current intensity. The scanning electron microscope (SEM) is a microscope that uses electrons instead of photons to form an image. This microscope, basically, consists of an electron gun and a set of electromagnetic fields to guide the electron beam toward the sample surface. Then, the beam scans the sample thanks to scanning coils. Finally, backscattered and secondary electrons received from the surface are collected by detectors and converted in a signal to produce the final image. Nowadays, the surface morphology of a solid sample can be studied by the SEM, because it has much higher resolution and has a large depth in field than a traditional microscope. On the other hand, in addition to the backscattered and secondary electrons from the sample surface, there are others types or signals produced during this process (Auger electrons, X-ray

fluorescence photons and others photons with various energies) that could be used in chemical analysis.

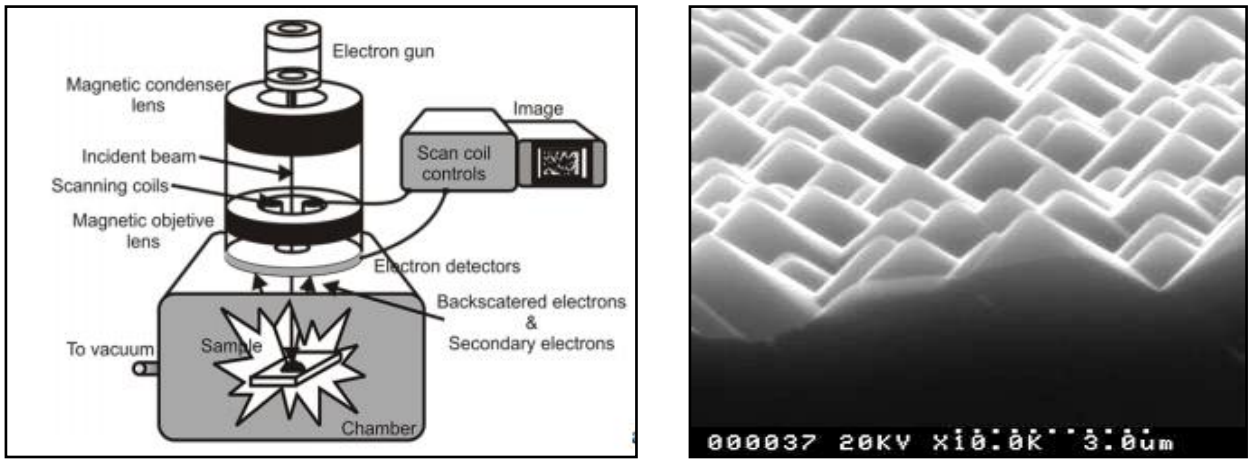

(a) (b)

Figure 4.3.(a)Scanning electron microscope (b), SEM image of randomly textured [3]

4.4.Light-Current-Voltage (LIV) Tester

LIV (Light-Current-Voltage) testing is done to evaluate the performance of the cell and mainly to calculate the efficiency of the solar cell. Initially the wafer is kept on the gold plated tray and then the bus bar of the cell is aligned with the pogo pins. Then the vacuum is turned on. Then the power supply and the control box are connected to the Laptop. LIV measurements using inexpensive, flash, xenon light source for illumination. LIV data acquisition is based on a custom-designed electronic interface integrated with high resolution, programmable voltage supply. Voltage across the solar cell is applied to measure the light generated photo-current. A user-friendly LabVIEW interface capable of writing data in ASCII format forms the basis of data acquisition. Spectral distribution of xenon high intensity plasma discharge lamp is light is closest to the solar spectra, and is industry standard. The flash LIV system is capable of measuring small (~ 10 cm^2) and large (up to ~15x15 cm^2) solar cells. The intensity variation is controllable in ~ 10 mW/ cm2 to 100 mW/ cm2 through simple absorptive metallic filters.

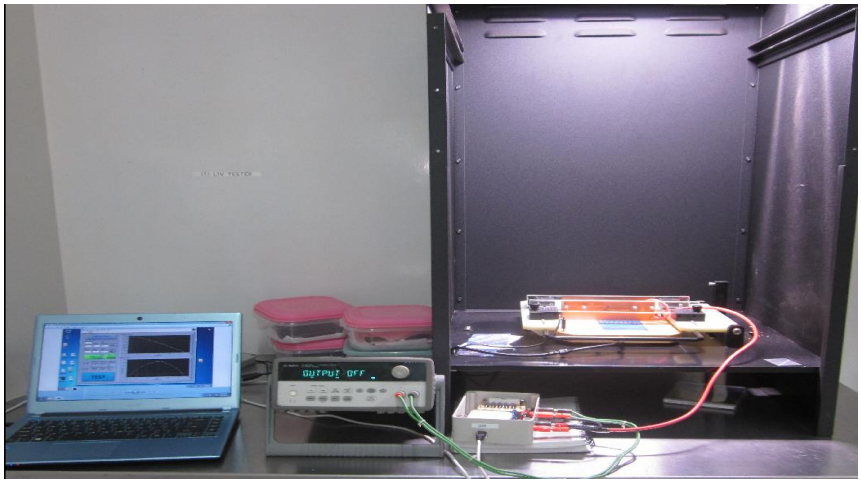

Figure 4.4. LIV measurement System [2]

Solar cells are characterized by their ability to convert sunlight into electricity. The light intensity (L)-current (I)-voltage (V) test is a series of measurements performed on complete solar cells to measure their operating characteristics. The LIV test identifies characteristics such as short circuit current (I_{sc}), open circuit voltage (V_{oc}), fill factor (FF) and maximum power (P_{max}). These results can be used to determine the efficiency of solar cell. Solar cells are tested under one-sun conditions using Xenon arc lamps; a xenon spectrum is closest to sunlight. Data acquisition based on programmable current-voltage source power supplies capable of handling current up to ~ 8 A is used in conjunction with a proprietary data acquisition system [2]. Calibration of this LIV measurements system is based on independently measured c-Si solar cells at Sandia National Laboratories.

4.5.Surface Photovoltage (SPV) Method

The surface photovoltage (SPV) method is a well-established contactless technique for semiconductor characterization that relies on analyzing illumination-induced changes in the surface voltage. Electrical properties of a free semiconductor surface are mainly determined by surface-localized electronic states within the semiconductor band gap or double layer of a charge, known as a surface dipole. The charge transfer between bulk and surface induced by the

appearance of surface-localized electronic states results in a non-neutral region named surface space charge region. If light falls on the pn-junction, the photons create electron-hole pairs separated by the space charge. Thus, in p-type silicon the majority carriers are holes, the charge in the depletion region is negative, and the electric field in the depletion region forces electrons to the surface, creating a surface photovoltage. Photons are absorbed not only in the pn-junction but also in the p-type area. The electrons produced are minority carriers in those areas and their concentration is greatly reduced by recombination.

The n-layer must therefore be sufficiently thin for the electrons of diffusion length L to pass through the n-layer. i.e, L >> t,
Where t = thickness of n-layer. [4]

When a typical 300μm thick silicon wafer is illuminated by strong sunlight of irradiance 1000 mW/cm^2, electrons and holes are generated at a rate of 9×10^{18} $cm^{-3}s^{-1}$[5] . The electric potential and the charge distribution are related to each other through the Poisson equation and the experimental value of the photo voltage coincides with the change of the surface potential. Minority carriers that drift around in the bulk either eventually recombine with majority carriers, or they reach the surface, where they produce a surface photovoltage. The shorter the diffusion length, the less likely minority carriers will make it to the surface to cause surface photo voltage. Longer wavelength light penetrates deeper into silicon than short wavelength light. Therefore, the longer wavelength will penetrate more deeply into the silicon, the minority carriers created will be more likely to recombine before they reach the surface and the longer wavelength light will produce a smaller SPV signal than the short wavelength light [7] .

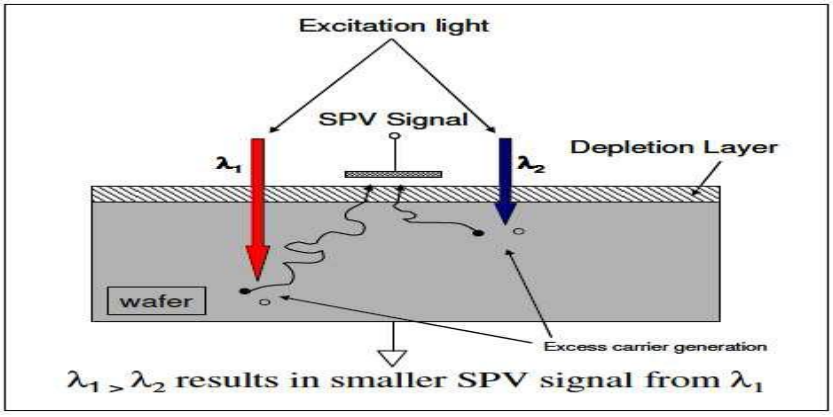

Figure 4.5. SPV Signal Changes with Penetration of incident light and wavelength

One can determine the diffusion length by comparing these two SPV signal produce by the two different wavelengths.

Figure 4.6. SPV Measurement System.

4.6.Four Point Probe

A four point probe is a simple apparatus for measuring the resistivity of semiconductor samples. By passing a current through two outer probes and measuring the voltage through the inner probes allows the measurement of the substrate resistivity. The doping concentration can be calculated from the resistivity using formulas.

The sheet resistivity of the top emitter layer is very easy to measure experimentally using a "four point probe". A current is passed through the outer probes and induces a voltage in the inner voltage probes. The junction between the *n* and *p* -type materials behaves as an insulating layer and the cell must be kept in the dark.

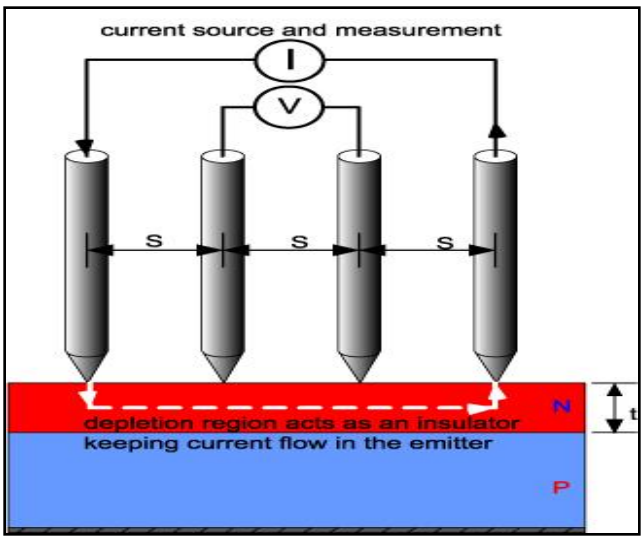

Figure 4.7. Resistance measurement by Four Point Probe

Using the voltage and current readings from the probe:

$$\rho_{\square}\left(\frac{\Omega}{\square}\right) = \frac{\pi}{ln\,(2)}\frac{V}{I}$$

Where:

$$\frac{\pi}{ln2} = 4.53$$

The typical emitter sheet resistivity of silicon solar cells lies in the range 30-100 Ω/□ .

In typical usage the current is set to 4.53 mA so that the resistivity is simply the voltage reading in mV.

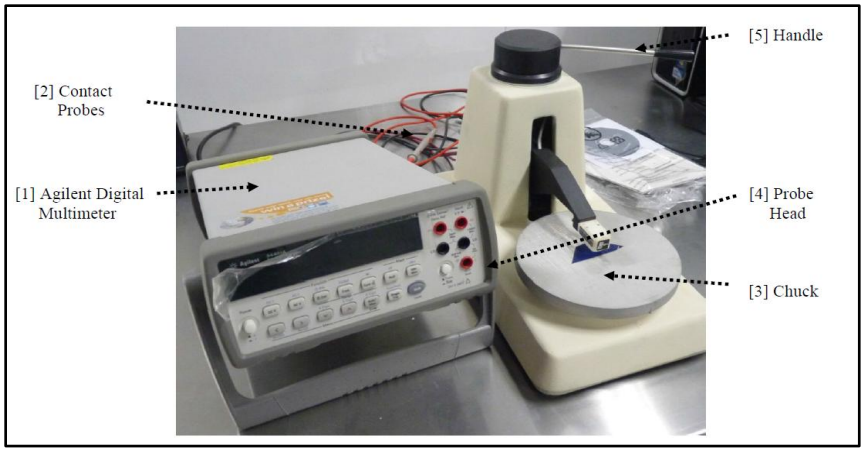

Figure 4.8. Four Point Probe

4.6.1. The Measurement of Bulk Resistivity

The measurement of bulk resistivity is similar to that of sheet resistivity except that a resistivity in cm^{-3} is reported using the wafer thickness, t:

$$\rho = \frac{\pi}{ln\,(2)} t \left(\frac{V}{I}\right) = 4.523t \left(\frac{V}{I}\right) \quad [9]$$

Where, *t* is the layer/wafer thickness in cm.

The simple formula above works for when the wafer thickness less than half the probe spacing ($t < s/2$). For thicker samples the formula becomes:

$$\rho = \frac{V}{I} \frac{\pi t}{ln\left(\frac{sinh\left(\frac{t}{s}\right)}{sinh\left(\frac{t}{2s}\right)}\right)}$$

4.6.2. Measuring Shunt Resistance (R_{SH}) and Series Resistance (R_S) from I_V Characteristics Curve

During operation, the efficiency of solar cells is reduced by the dissipation of power across internal resistances. These parasitic resistances can be modeled as a parallel shunt resistance (R_{SH}) and series resistance (R_S).

For an ideal cell, R_{SH} would be infinite and would not provide an alternate path for current to flow, while R_S would be zero, resulting in no further voltage drop before the load.
Decreasing R_{SH} and increasing R_s will decrease the fill factor (FF) and P_{MAX} as shown in Figure 4.9. If R_{SH} is decreased too much, V_{OC} will drop, while increasing R_S excessively can cause I_{SC} to drop instead.

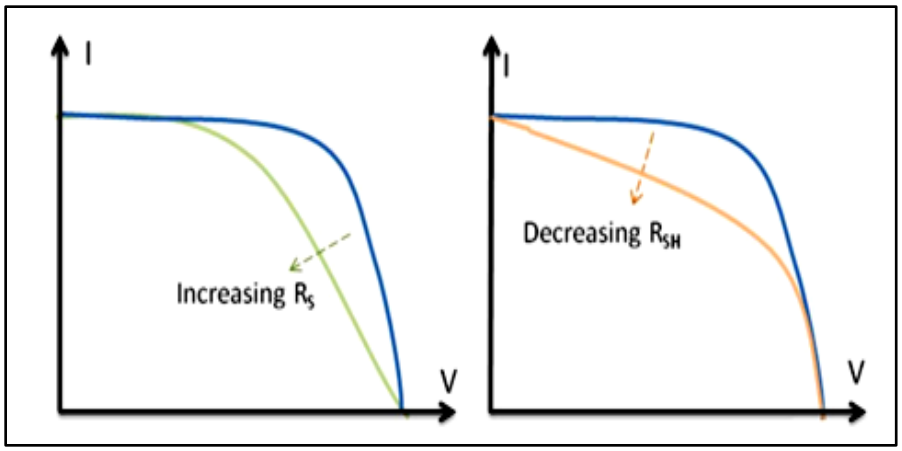

Figure 4.9. Effect of Diverging R_s & R_{SH} from Ideality [9]

It is possible to approximate the series and shunt resistances, R_S and R_{SH}, from the slopes of the I-V curve at V_{OC} and I_{SC}, respectively. The resistance at V_{oc}, however, is at best proportional to the series resistance but it is larger than the series resistance. R_{SH} is represented by the slope at I_{SC}. Typically, the resistances at I_{SC} and at V_{OC} will be measured and noted, as shown in Figure 4.10.

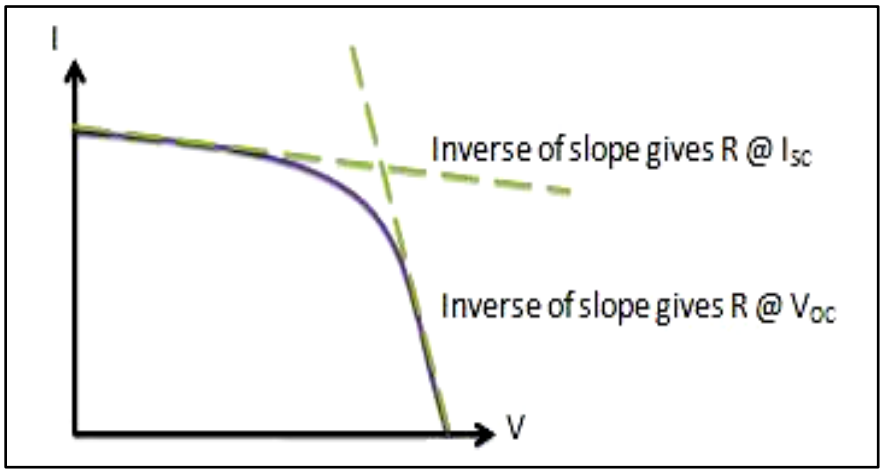

Figure 4.10. Obtaining Resistances from the I-V Curve [9]

References

[1] Instruction Manual Spectral Reflection and Response Measurement System, Institute of Electronics, Atomic Energy research Establishment, Savar.

[2] Instruction Manual Flash LIV Solar Cell Tester, Institute of Electronics, Atomic Energy research Establishment, Savar.

[3] W. H. Southwell, Opt. Lett. 8, 584 (1983)

[4] J. Toušek, D. Kindl, J. Touškova, "Contactless photovoltage method for measurement of diffusion length of minority carriers in solar cells", Solar Energy Materials & Solar Cells, 64, p. 29-35, 2000.

[5] A. Cuevas, D. Macdonald, "Measuring and interpreting lifetime of silicon wafers", Solar Energy 76 (2004) 255-262.

[6] L. Kronik, Y. Shapira, "Surface photovoltage phenomena: theory, experiment, and applications", Surface science, report 37, p. 1- 206, 1999.

[7] Instruction Manual Four Point Probe System, Institute of Electronics, Atomic Energy research Establishment, Savar.

[8] http://PVeducation.org/PVcdrom/solar-cell-operation/effect-of-parasitic-resistances.

Chapter 5

Result and Analysis

Part A

5.1.Solar Photovoltage (SPV) Measurement

Solar cells are characterized by their ability to convert sunlight into electricity. For high efficiency solar cells, adequate surface passivation and high minority carrier lifetime are required. For p-type doped Si wafers, a simple method based on surface photovoltage (SPV) has been developed. This SPV minority carrier lifetime measurement system has been designed to characterize up to 6-inch diameter Si wafers. A computer-controlled monochromator illuminates the wafer under test over a broad (500-1000 nm) spectral range. Surface photovoltage generated by incident light is measured through a lock-in amplifier to provide detection capability over extremely large (μV to V) scale. A LabVIEW-based computer interface is used to acquire SPV as a function of wavelength. A linear regression analysis of the plotted data provides the wafer minority carrier lifetime. For short wavelength ranges, method also provides qualitative information on surface passivation.

5.2.SPV Method Description

The surface photovoltage (SPV) technique utilizes the change of the electrochemical potential in the space-charge region of a semiconductor during excess carrier generation due to illumination of the sample with light of suitable wavelength and intensity [1]. The SPV method is a well-established contactless technique for the non-destructive characterizations of semiconductors bulk materials, multi-layers, nanostructures, and actual devices [2]. In 1961, Goodman showed that, under certain assumption, by making measurements of SPV as a function of wavelength, the minority carrier diffusion length can be determined. Therefore, the primary of the SPV technique is the determination of the diffusion length of minority carriers in the region of essential light absorption inside solar cells and wafers under dc conditions [3].

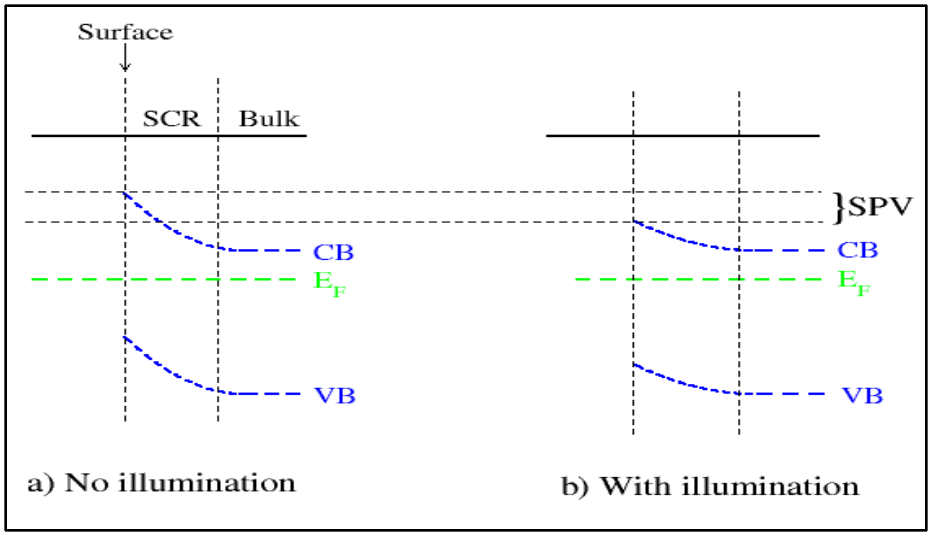

Figure 5.1. Change in surface potential without (a) and with light illumination (b)

5.3.Minority Carrier Diffusion Length & Lifetime

The minority carrier diffusion length, L is essential for evaluation of the quality and transport properties of the material. In the base region, the diffusion length is a critical factor impacting the conversion efficiency and spectral response of the cell. The SPV is generated when some of the minority carriers that drift around in the bulk reach the surface. The statistical distance that carriers travel in the bulk before they recombine is the diffusion length. Since, some of the minority carriers recombine before they reach the surface, therefore, the shorter the diffusion length, the smaller the SPV signal due to the high recombination losses.

SPV measurements require measurement of the potential of a semiconductor surface subjected to light incidence. The surfaces of semiconductors are often depletion (or space charge) regions where the built-in electric field due to defects or junction formation has transported all free charge carriers. A reduced carrier density means that the electronic energy band of the majority carriers is bent away from the Fermi level (Fig. 4.1). This band-bending is responsible for the surface potential. Photo-generated electron-hole pairs, generated within the semiconductor, diffuse through the bulk of the sample before reaching the surface depletion region. The photo-

generated minority carriers have a shorter diffusion length than the much more numerous majority carriers, with which they can combine radiativley. Therefore, the change in surface potential on exposure to light is an indicator of the ability of minority carriers to reach the surface, i.e., the minority carrier diffusion length.

The diffusion length, *L*, is approximately related to the minority carrier lifetime $\tau_{bulk}$by

$$L = (D \times \tau_{bulk})^{1/2}$$

Where *D* is the diffusion coefficient. Note that the diffusion length, *L*, is independent of any built-in fields in contrast to the drift behavior of the electron-hole pairs. Another important factor to note is that while the photo-generated majority carriers also diffuse towards the surface, however, their number, as a fraction of the thermally generated majority carrier density in a moderately doped semiconductor, is far too small to create any significant, measurable photovoltage. Both types of photo-generated carriers also diffuse towards the rear surface where their collection can introduce errors in data interpretation particularly when the diffusion lengths are larger than the wafer thickness.

In real semiconductors, the measured diffusion length,

$$L_{mean} = \sqrt{(D \times \tau_{eff})},$$

includes the effect of surface recombination, which is best understood through its effect on carrier lifetime:

$$1/\tau_{eff} = 1/\tau_{bulk} + 2 \times s/d$$

Where τ_{eff} is the effective minority carrier lifetime, τ_{bulk} is the bulk minority carrier lifetime, s is the surface recombination velocity, and d is the wafer thickness. Even for well characterized materials, uncertainty regarding the actual value of the surface recombination velocity reduces the accuracy with which the diffusion length can be determined.

5.4.Experimental SPV Setup

A simple, computer-controlled, normal incidence measurement system was designed for SPV measurements of minority carrier lifetime of Si and other semiconductor wafers. Measurement system is based on a mini monochromator driven with a stepper motor to vary wavelengths in ~ 500-1200-nm spectral range. Light-induced surface photovoltage (SPV) is measured as a function of the wavelength. SPV is measured using a Stanford Research 510 lock-in amplifier. This system can be modified to measure SPV as a function of wavelength as well as a function of flux density at fixed wavelength. A LabVIEW interface is used for system control and data acquisition.

The figure below describes detailed system schematics of the minority carrier lifetime measurement system that includes:

1. 150W fibre optical microscopic illuminator
2. Motorized Mini monochromator
3. Stepper motor
4. Aurum coated wafer chunk
5. Ito/Aurum coated quartz plate
6. Light chopper
7. Vacuum pump
8. Contact probe
9. Stanford research 510 lock-in amplifier
10. National Instruments USB 6008

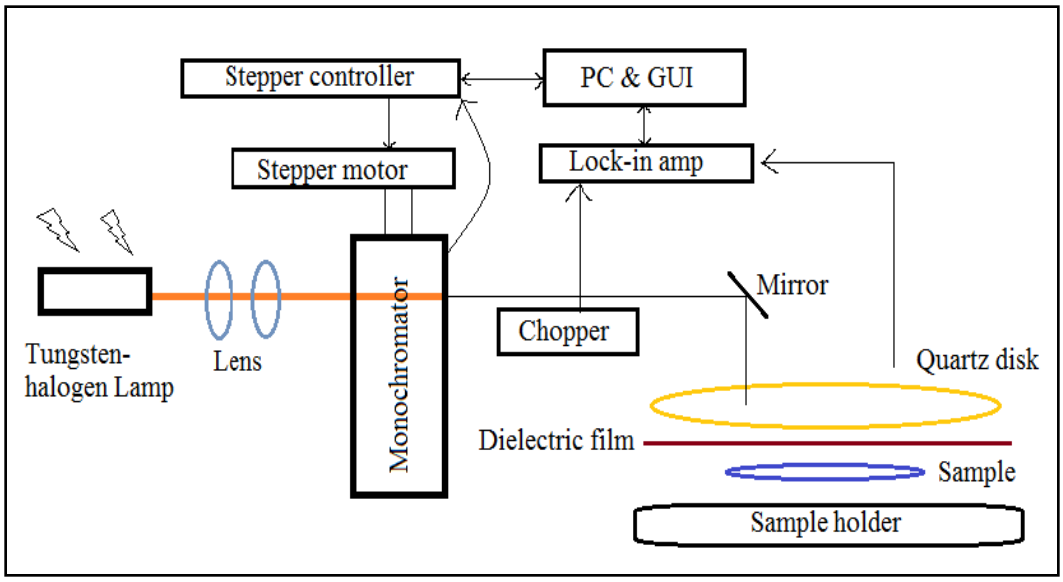

Figure 5.2. Basic block diagram of the SPV measurement

5.4.1. Mini Mono-Chromator

Motorized monochromator use a stepping motor driven by an external motor controller with RS 232 interface. Included with the controller is an application program with over 25 commands to control a variety of operations of the grating drive. These motorized models also include a manual drive and a digital counter that displays the wavelength to 0.2 nm.

These new monochromators are low cost, compact and simple-to-use instruments for moderate resolution applications. They are ideal for general laboratory experiments and educational studies covering fixed wavelength ranges and not requiring sub-nanometer resolutions.

Light from a tungsten-halogen lamp is focused onto the entrance slit of the monochromator (Fig. 5.3). The output from the monochromator is directed to the wafer vacuum chuck with a simple folding mirror. During normal operation, light from the exit slit of the monochromator is guided to the wafer at normal incidence.

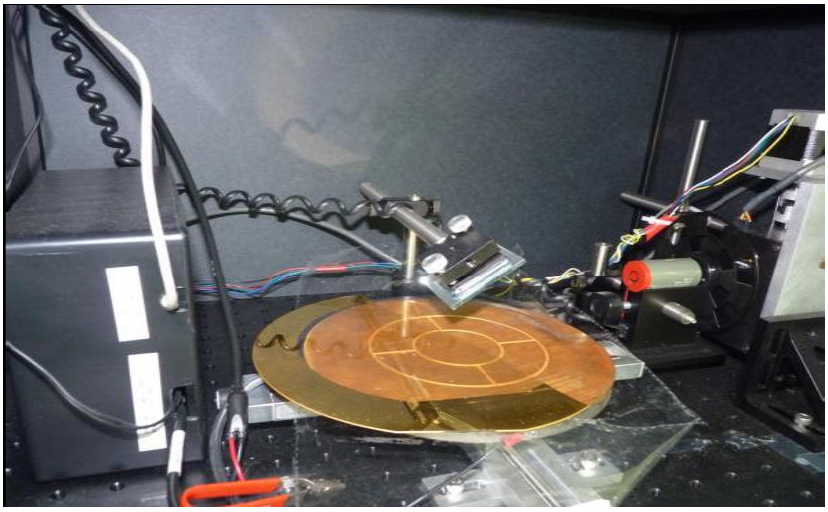

Figure 5.3. Close-up views of the SPV system showing wafer chuck, interface box, and the folding mirror

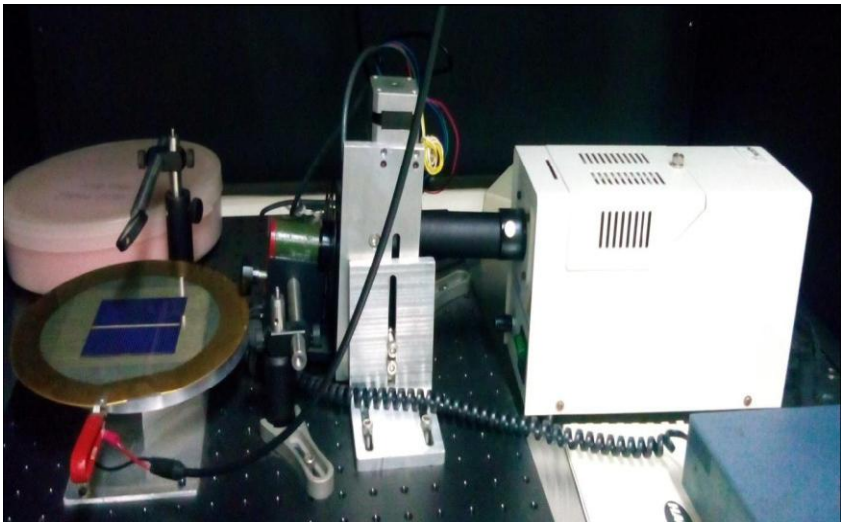

Figure 5.4. 150W fibre optical microscopic illuminator, Motorized monochromator,

5.4.2. Stepper Motor

A stepper motor is an electromechanical device which converts electrical pulses into discrete mechanical movements. The shaft or spindle of a stepper motor rotates in discrete step increments when electrical command pulses are applied to it in the proper sequence. The motors

rotation has several direct relationships to these applied input pulses. The sequence of the applied pulses is directly related to the direction of motor shafts rotation. The speed of the motor shafts rotation is directly related to the frequency of the input pulses and the length of rotation is directly related to the number of input pulses applied.

Stepper motor is used to vary monochromator output wavelength. Monochromator wavelength calibration is determined through electronic upper and lower limit switches. These limit switches are determined by moving the stepper motor to the limit switch. For example, the upper limit switch for this monochromator is set at 1205.7 nm and the lower at ~ 28 nm. Once the system finds the limit switch, wavelength is defined, and system is moved to desired wavelength by setting up known number of steps.

5.4.3. SR510Lock-in Amplifier

The Lock-in technique is used to detect and measure very small ac signals. A Lock-in amplifier can make accurate measurements of small signals even when the signals are obscured by noise sources which may be a thousand times larger. Essentially, a lock-in is a filter with an arbitrarily narrow bandwidth which is tuned to the frequency of the signal. Such a filter will reject most unwanted noise to allow the signal to be measured. A typical lock-in application may require a center frequency of 10 KHz and a bandwidth of 0.01 Hz. This 'filter' has a Q of 106 -well beyond the capabilities of passive electronic filters.

In addition to filtering, a lock-in also provides gain. For example, a 10 nanovolt signal can be amplified to produce a 10 V output--a gain of one billion.

All lock-in measurements share a few basic principles. The technique requires that the experiment be excited at a fixed frequency in a relatively quiet part of the noise spectrum. The lock-in then detects the response from the experiment in a very narrow bandwidth at the excitation frequency.
The lock-in output and stepper motor are controlled by a PC using a LabVIEW interface. The system wavelength range is from ~ 500-1200-nm. All data is written to a file in text form for subsequent plotting and processing.

Figure 5.5. Stanford research 510 lock-in amplifier.

The table below lists some specifications for the SR510 lock-in amplifier. Also listed are the error contributions due to each of these items. The specifications will allow a measurement with a 2%accuracy to be made in one minute. We have chosen a reference frequency of 5 kHz so as to be in a relatively quiet part of the noise spectrum. This frequency is high enough to avoid low frequency '1/f' noise as well as line noise. The frequency is low enough to avoid phase shifts and amplitude errors due to the RC time constant of the source impedance and the cable capacitance.

The full-scale sensitivity of 100 nV matches the expected signal from our sample. The sensitivity is calibrated to 1%. The instrument's output stability also affects the measurement accuracy. For the required dynamic reserve, the output stability is 0.1%/°C. For a 10°C temperature change we can expect a 1% error.

A front-end noise of 7 nV/√Hz will manifest itself as a 1.2 nVrms noise after a 10 second low-pass filter since the equivalent noise bandwidth of a single pole filter is 1/4RC. The output will converge exponentially to the final value with a 10 second time constant. If we wait 50 seconds, the output will have come to within 0.7% of its final value [4].

The dynamic reserve of 60 dB is required by our expectation that the noise will be a thousand times larger than the signal. Additional dynamic reserve is available by using the band pass and notch filters. A phase-shift error of the PLL tracking circuits will cause a measurement error equal to the cosine of the phase shift error. The SR510's 1° phase accuracy will not make a significant contribution to the measurement error.

Table 5.1. Specification of Lock in Amplifier

Accuracy	20%
full-scale sensitivity	100 nV
output stability	0.1%/°C
dynamic reserve	60B

5.4.4. Light chopper

A light chopper is placed at the exit slit of the monochromator to provide reference signal to the lock-in to ensure all the stray light is rejected by the system and enhance system sensitivity from nanovolt to mV range.

The Model SR540 Optical Chopper is used to square-wave modulate the intensity of optical signals. The unit can chop light sources at rates from 4 Hz to 3.7 kHz. Versatile, low jitter reference outputs provide the synchronizing signals required for several operating modes: single or dual beam; sum & difference frequency; and synthesized chopping to 20 kHz.

Specifications

Table 5.2. Specification of Light chopper

Chop Frequency	4 Hz to 400 Hz with 6 slot blade. 400 Hz to 3.7 kHz with 30 slot blade.
Frequency Stability	250 ppm/°C typical.
Long Term Frequency Drift	< 2%, 100 Hz < f < 3700 Hz
Phase Jitter	0.2° rms from 50 Hz to 400 Hz.

	0.5° rms from 400 Hz to 3.7 kHz
Frequency Display	4 digit, 1 Hz resolution, 1 Hz accuracy
Frequency Control	10 turn pot with 3 ranges: 4 Hz to 40 Hz 40 Hz to 400 Hz 400 Hz to 3.7 kHz
Dimensions	Controller 7.7" x 5.1" x 1.8" Chopper Head 2.8" x 2.1" x 1.0" Blade Diameter 4.00"
Power	100 / 120 / 220 / 240 VAC 50 / 60 Hz 12 watts

5.4.5. ITO/Au Coated Quartz Plate

Capacitive SPV voltage is measured by placing an ITO/Au coated quartz plate on top of the wafer to be measured. A thin-sheet of Teflon film is placed between the top glass electrode and the wafer to create electrical isolation. The bottom electrode is connected to the Si wafer and is Au-coated to provide reduced contact resistance.

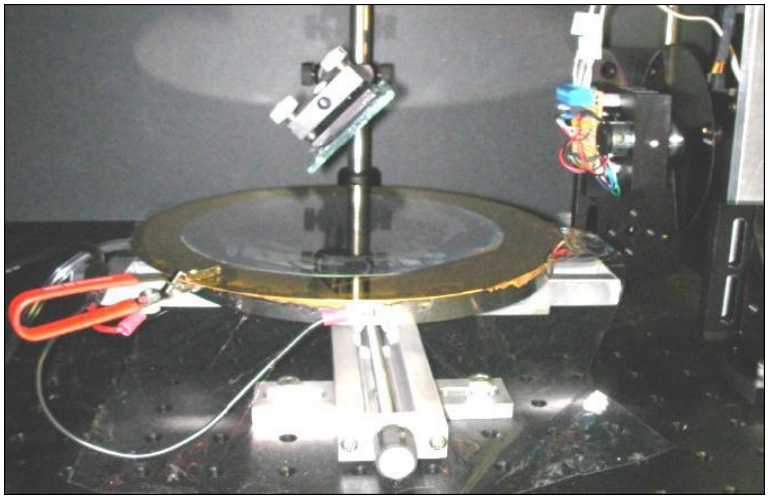

Figure 5.6. The wafer under test sandwiched between the Au-coated chuck and ITO-coated quartz plate with Au-coated contacts at boundaries (right).

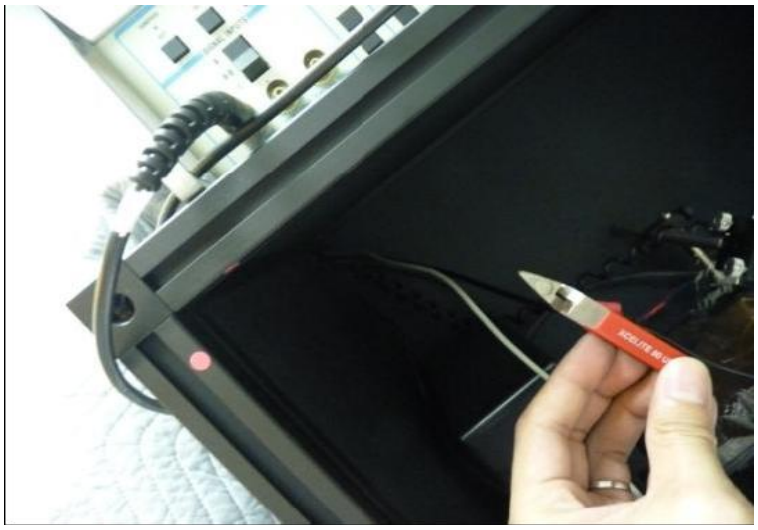

Figure 5.7. Close-up views of the contact for Au/ITO-coated quartz plate (left)

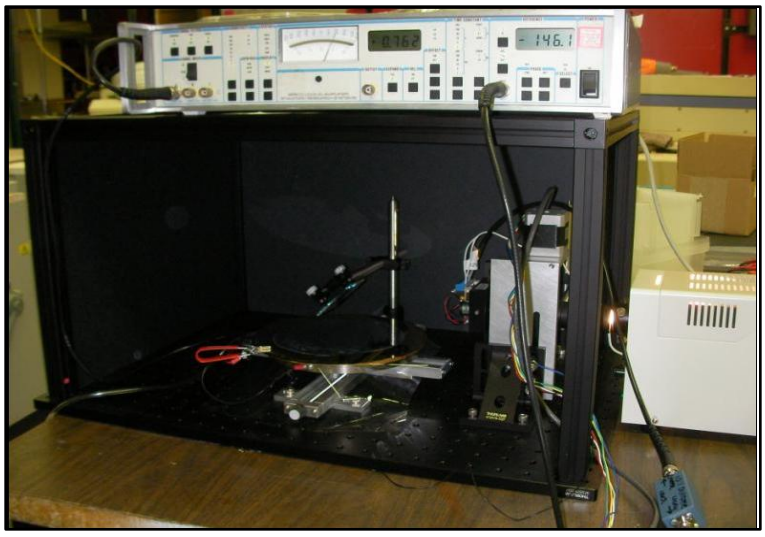

Figure 5.8. Working SPV system with lock-in exhibiting signal of 0.74 and frequency of 146 Hz.

5.4.6. Setup Procedure on Computer Data Acquisition

Prior to data acquisition, settings on the lock-in amplifier are manually set. This is done by looking at the SPV signal at wavelength of ~ 600 nm (red light).

Following lock-in settings are fairly standard for these measurements:

(a) chopper frequency in ~ 30-200 HZ range,

(b) time constant ~ 100-300 ms,

(c) all input filters engaged,

(d) dynamic resolution off,

(e) offset off, and voltage scale is set anywhere between ~ 0.2 mV to 2 mV.

Once the lock-in settings are set, LabVIEW interface is used to acquire data by following the steps outlined below.

i. Stepper motor speed is input; typically between 50-100 nm/min,

ii. Stepper motor is moved until upper limit switch corresponding to a wavelength of ~ 1205.7 nm is detected,

iii. Desired initial (λi) and final (λf) wavelengths are input for lifetime measurement scans,

iv. Incremental wavelength step (λs) in nm is input,

v. At each wavelength position, SPV signal is acquired from the lock-in amplifier,

vi. Computer program calculates total number N of SPV measurements;

$$N = [\ (\lambda f - \lambda i)/\lambda s\ ]$$

vii. Computer moves stepper motor by increments of $(400/75)*\lambda$ ssteps for each of the wavelength measurements,

viii. Computer program measures SPV at each wavelength $(\lambda j)=\lambda i+(\lambda f-\lambda i)*j/N$, where N is the total number of measurements defined above, and j is each individual measurement,

ix. Once scan is completed, computer program writes the data file with two columns ($\lambda(j)$, V(j)),

x. After the file, if more scans are needed, procedure from steps i. through steps ix are repeated, and finally

xi. If all data acquisition is completed, system requests that the wavelength be set at λ=600 nm so that alignment is visually convenient for next set of measurements.

In order for this setup to work a computer must be connected to see the digital result. The block diagram below shows how these two figures are connected practically:

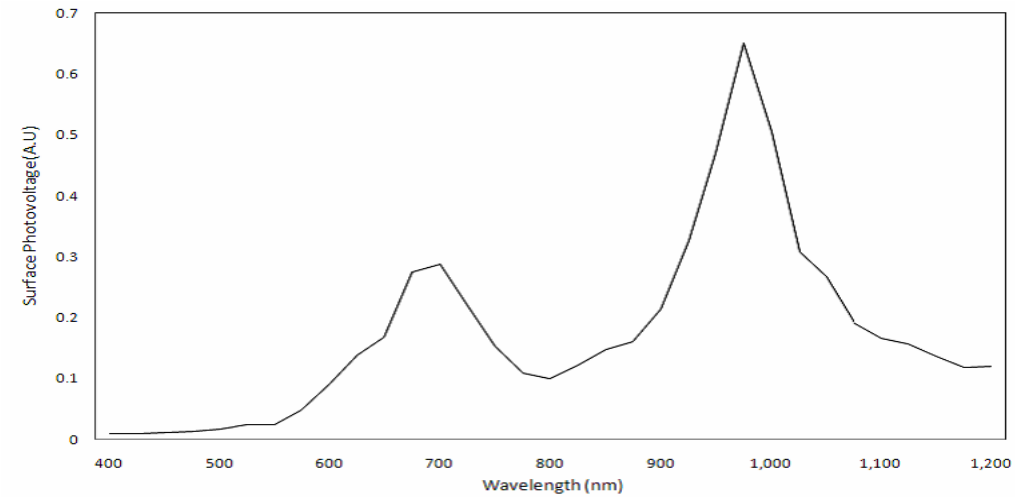

Figure 5.9. The form of graph displayed, where λ-SPV is plotted.[5]

With the help of this displayed data (ideal), a reciprocal of α versus reciprocal of spv is plotted which ideally looks like:

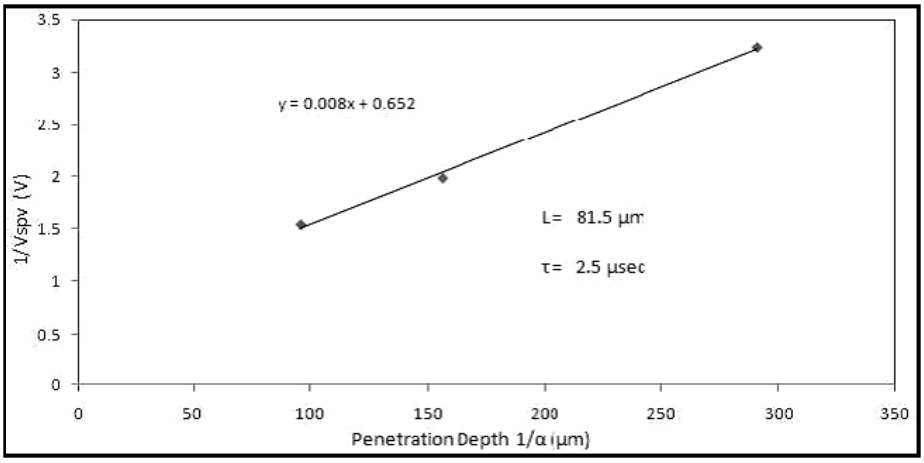

Figure 5.10. The ideal form of penetration depth versus 1/Vspv graph that is plotted with the help of data in Fig. 5.9.[5]

This graph is used to find the value of diffusion length that is found by its x-intercept.

5.5. Experimental Results

LAB VIEW results shows the SPV results in arbitrary unit. Table 5.3. Data obtained from the SPV measurement system and corresponding data for plotting graph.

Table 5.3. Data obtained from the SPV measurement system

Wavelength (nm)	VSPV (V)	alpha/cm	Reciprocal of α [x]	1/Vspv
400.0	0.008752	9.52E+04	1.05E-01	114.2596
420.0	0.011230	5.00E+04	2.00E-01	89.0472
440.0	0.010170	3.11E+04	3.22E-01	98.32842
460.0	0.016369	2.10E+04	4.76E-01	61.09109
480.0	0.100115	1.48E+04	6.76E-01	9.988513
500.0	0.011408	1.11E+04	9.01E-01	87.65778
520.0	0.011352	8.80E+04	1.14E-01	88.0902
540.0	0.009894	7.05E+03	1.42E+00	101.0714
560.0	0.012030	5.78E+03	1.73E+00	83.12552
580.0	0.016497	4.88E+03	2.05E+00	60.61708
600.0	0.009456	4.14E+03	2.42E+00	105.753
620.0	0.009690	3.52E+03	2.84E+00	103.1992
640.0	0.009726	3.04E+03	3.29E+00	102.8172
660.0	0.010858	2.58E+03	3.88E+00	92.09799
680.0	0.016135	2.21E+03	4.52E+00	61.97707
700.0	0.026755	1.90E+03	5.26E+00	37.37619
720.0	0.057274	1.66E+03	6.02E+00	17.45993
740.0	0.108288	1.42E+03	7.04E+00	9.234634
760.0	0.161041	1.19E+03	8.40E+00	6.209599

780.0	0.246863	1.01E+03	9.90E+00	4.05083
800.0	0.312239	8.50E+02	1.18E+01	3.202675
820.0	0.341902	7.07E+02	1.41E+01	2.924815
840.0	0.417073	5.91E+02	1.69E+01	2.397662
860.0	0.276158	4.80E+02	2.08E+01	3.621115
880.0	0.216894	3.83E+02	2.61E+01	4.610547
900.0	0.132755	3.06E+02	3.27E+01	7.532673
920.0	0.108309	2.40E+02	4.17E+01	9.232843
940.0	0.149111	1.83E+02	5.46E+01	6.706413
960.0	0.087267	1.34E+02	7.46E+01	11.45909
980.0	0.069836	9.59E+01	1.04E+02	14.31926
1000.0	0.106754	6.40E+01	1.56E+02	9.36733

From the testing of SPV we get the following graphs

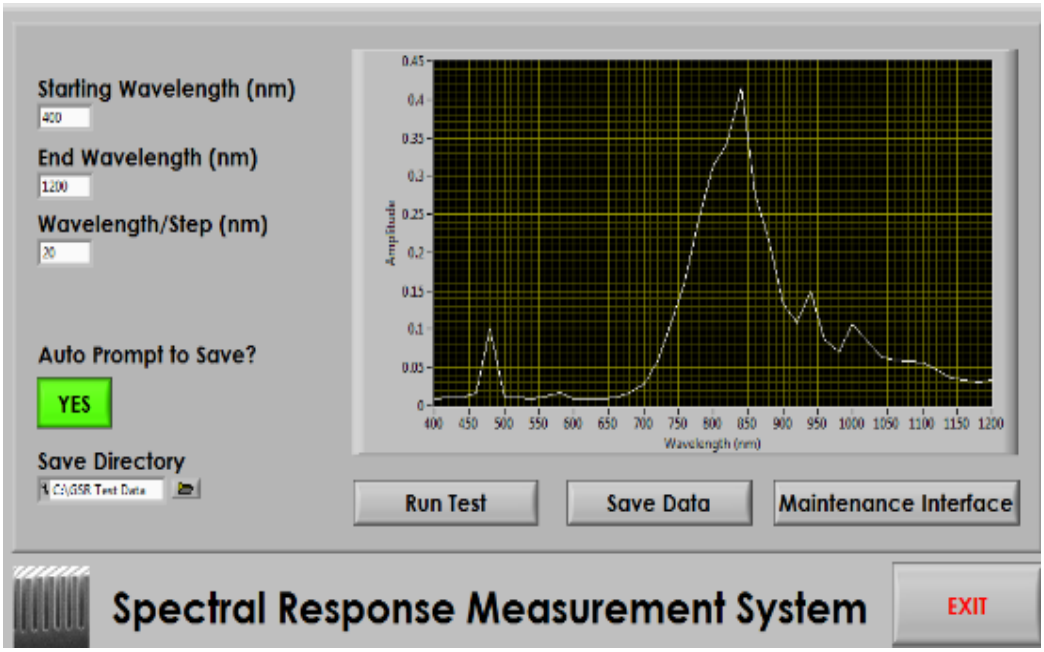

Figure 5.11. The LabVIEW Image

Figure 5.11 plotted by using the data shown in Table 5

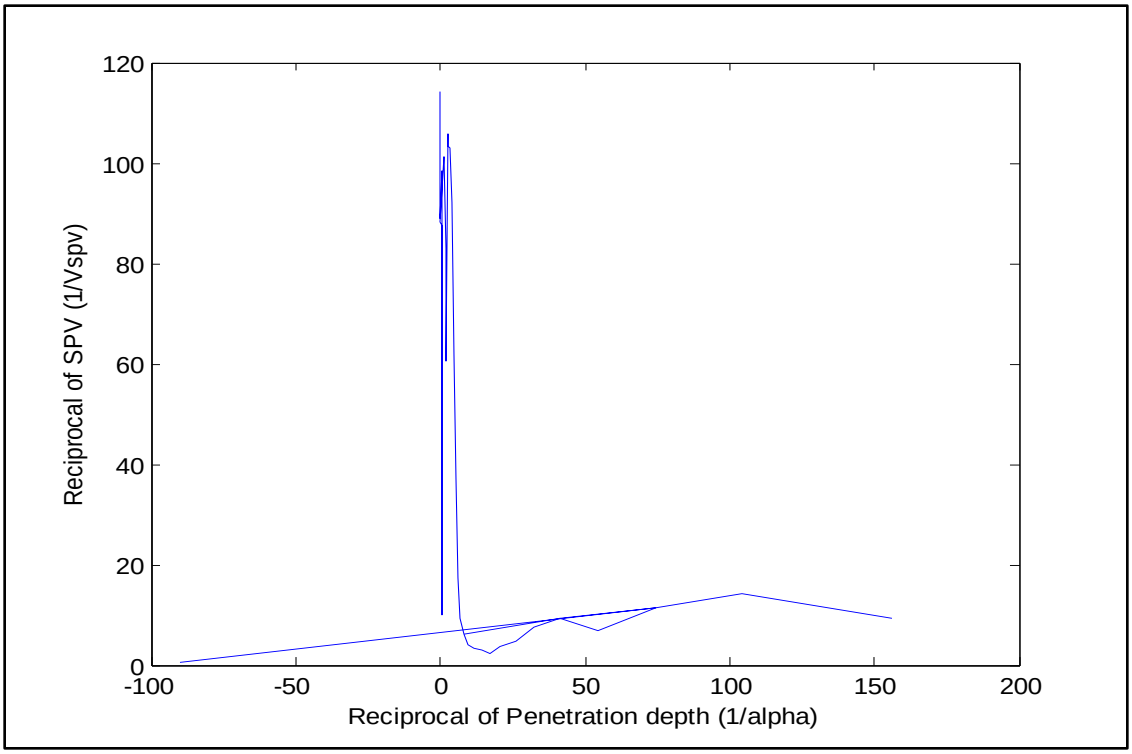

Figure 5.12. 1/alpha v_s 1/Vspv represents minority carrier diffusion length

This figure (5.12) is plotted in MATLAB and the code is given in appendix 2. This figure is used to find the value of diffusion length that is found by its –x intercept and the value is 92 μm.

Equation of minority carrier diffusion length:

$$L_n = \sqrt{D\tau_n}$$

Where this Ln is the diffusion length, D is the diffusivity (for Si D= 27 cm^2/s), and τ is the lifetime.

Minority carrier lifetime becomes

$$\tau_n = \frac{L_n^2}{D} = 3.135\ \mu s$$

5.6.Discussion

The SPV data was plotted as a function of 1/α. The minority carrier diffusion length for cell surface was determined to be 92 μm. For Si minority carrier diffusion coefficient, *D*, to be 27 cm2/sec; the effective lifetime for sample cell is 3.135μsec. The main challenge of SPV measurement was to calibrate the system. At first the light emitted from the monochromator must focused on the mirror properly and the second challenge was to set the sensitivity of lock in amplifier so that the peak of the curve doesn't cut and get the full curve in range of selected wavelength.

Part B

5.7. Efficiency Measurement and I-V Characteristic

Solar cells are characterized by their ability to convert sunlight into electricity. This solar cell efficiency measurement using sun simulator system determines fundamental device characteristics including short circuit current (Isc), open circuit voltage (Voc), fill factor (FF), series resistance (Rs), shunt resistance (R_{SHUNT}), and maximum power (Pmax). Those collected results, can be used to determine the efficiency of solar cell. Incident intensity is controllable using absorptive metallic filters. System is independently calibrated with pre-qualified solar cells.

Efficiency is the ratio of output to input; in case of solar cell energy conversion we call this value η. This is the percentage of solar energy to which the cell is exposed that is readily being converted to electrical energy. The value of η can be calculated by:

Solar Cell Efficiency, $\eta = FF*V_{OC}*I_{SC}/(E*A)$

Where E is the input light energy in W/m^2, and A is the surface area of the solar cell in m^2.

Generally this I-V characteristic would fall under electrical characterization, however since the measurement is usually taken by sun or sun-simulator i.e. optically induced; this is also an optical characterization.

5.8.Experimental Setup for Efficiency Measurement

The sun simulator is essentially a solar cell I-V measurement system that consists of multiple components such as the K201 solar simulator, K101 photovoltaic power meter, K401 solar simulator power supply, K202 auto controller, K901 sample mounting jig and K730 the software that measures the IV characteristics. The full system of sun simulator describes in Appendix 1.

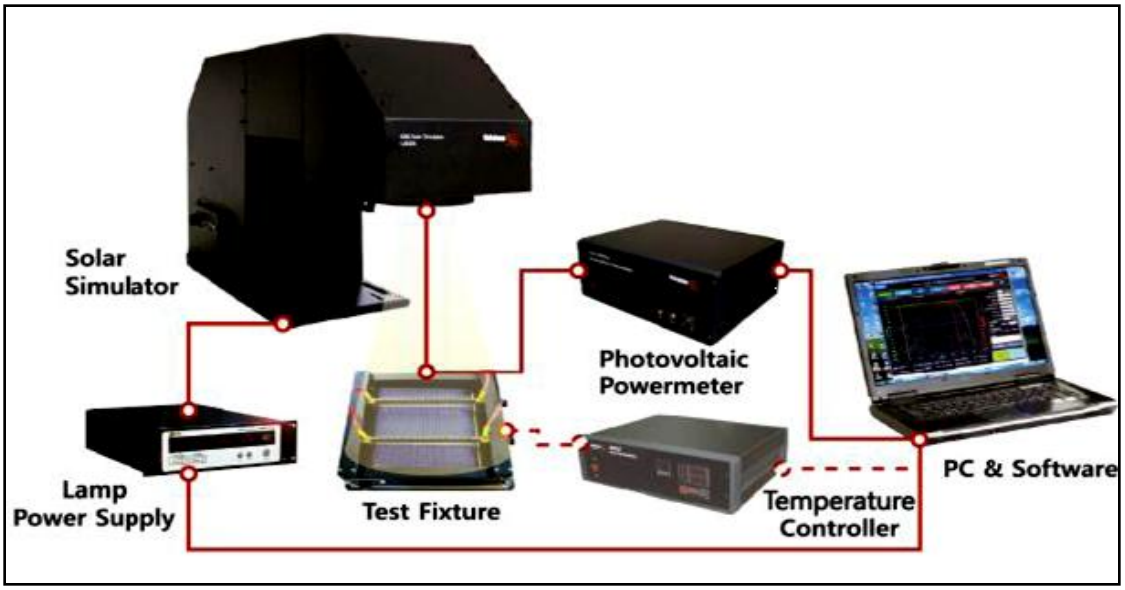

Figure 5.13. Complete setup of the system [6].

This system, shown in fig.5.13, is generally meant for the IV measurement of thin films, however due to the flexible mounting jig—measurement of our sample i.e. simple wafer is also possible. For the ideal output a K801 reference cell is used.

5.8.1. Specification of Reference Cell (K801)

Table 5.2 Specification of Reference Cell (K801)

Specification	Value
Irradiance Monitoring and Calibration Spectral Range	350 nm ~ 1,100 nm
BK7 Filter for C-Si Cell	
KG5 Filter for DSSC	

5.9.Equation for Measuring the Solar Cell Efficiency

In order to measure solar cell performance, the positive and negative probes are connected to an electronically-controlled resistive system. As the voltage across the solar cell is varied, current flow across the load resistor goes from zero to a maximum value (short-circuit). Maximum power is achieved at a point often referred to as the maximum power point (MPP) at which the product $P=V*I=V_m*I_m$ is at its maximum value. The ratio of V_m*I_m to $V_{OC}*I_{SC}$ is defined as the solar cell fill factor (FF).

Solar Cell Fill Factor (FF) = $V_m*I_m / V_{OC}*I_{SC}$……(1)

FF is a complicated function of many variables including resistance, minority carrier lifetime, surface recombination; it usually in the ~ 0.6-0.8 range, higher FF represents higher efficiency solar cell.

There are several ways through which solar cell efficiency can be measured; simplest method is described here. Solar cell efficiency is simply described as the ratio of output power to input power, i.e.,

Solar Cell Efficiency (η)= cell output/ input energy ……(2)

From Eq. (1), cell output is given by

Solar Cell Output=Vm*Im= $FF*V_{OC}*I_{SC}$…….....(3)

Peak solar cell incident solar radiation is considered to be 100 mW/cm^2. This is also referred to as AM 1.5 solar insolation; all terrestrial efficiency measurements refer to AM 1.5. Therefore, for AM 1.5 illumination, on can rewrite equation (2) as follows:

Solar Cell Efficiency (η)=$FF*V_{OC}*I_{SC}/(0.1*A)$…… ……(4)

In eq. (4), A is solar cell area is in cm2, V_{OC} is in V, and I_{SC} is in A.

From Eq.(4), I_{SC} is then given by

$I_{SC}=(\eta*0.1*A)/(FF*V_{OC})$ ……(5)

5.10. Experimental Result

For conducting the experimental study, we have we have choose a reference cell from India of 156 cm^2 monocrystalline silicon solar cell, which has been placed on the jig of solar simulator's (Sun Simulator K3000 LAB55) platform at 25^oC. Xenon lamp of sun simulator produced light of input power 100$mWcm^{-2}$. Before taking the result from the solar simulator, calibration has been done with respect to a reference cell. The vertical position of the reference cell has been adjusted such that the major performance parameters of the cell obtained from the simulator match exactly to its specification sheet.

By using sun simulator, we have measured the efficiency for different areas of same solar cell and analysis the changes of data for different areas of solar cell which indicate that the whole area of solar cell is almost uniformed.

From sun simulator, we have obtained the following results which are presented in the table 5.5 below.

Table 5.5. Results from Sun Simulator

Test	**Area cm^2**	**Voc (V)**	**Isc (mA)**	**Jsc (mA/cm^2)**	**P_{max} (mW)**	**V_{max} (V)**	**I_{max} (mA)**	**Fill Factor (%)**	**Efficiency (%)**	**R Shunt (Ohm)**	**R Series (Ohm)**
1	10.24	0.609	595.678	58.172	164.381	0.357	459.87	45.35	16.05	20.542	0.495
2	10.24	0.611	598.187	58.417	164.878	0.365	451.82	45.09213	16.10	14.338	0.494
3	9	0.599	604.619	67.18	148.995	0.337	442.66	41.11	16.55	6.184	0.542

We draw the I-V curve and P-V curve for test 1 data. From the table 5.5 we observed that the efficiency for different we can say that the cell is well fabricated.

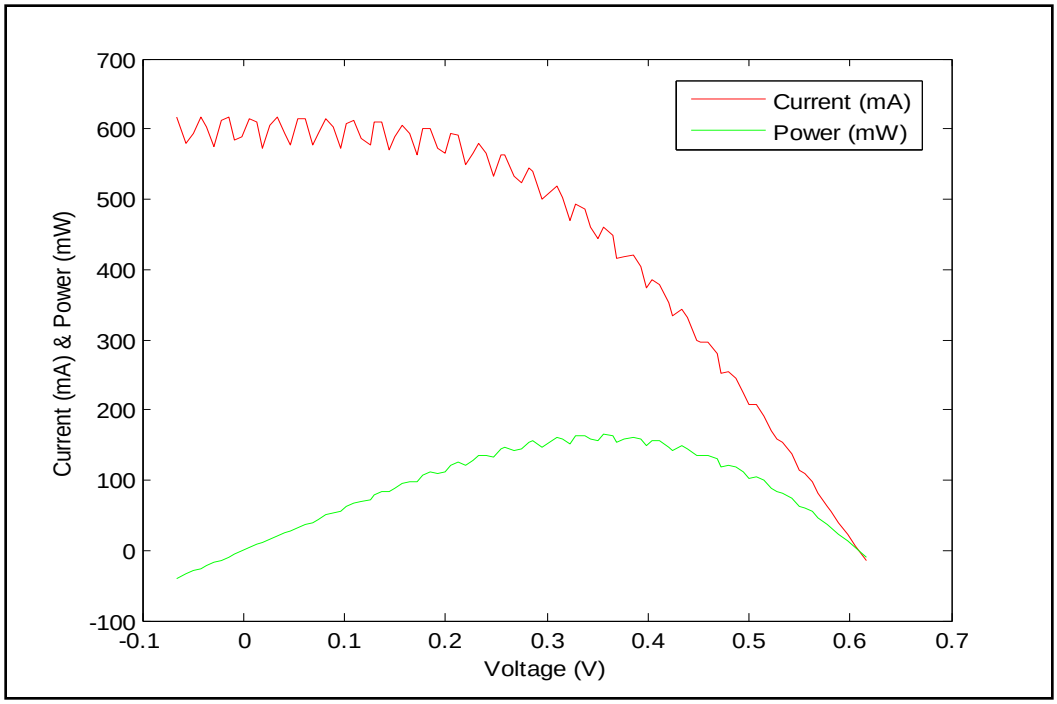

Figure 5.16. 1 I-V Characteristics Curve of Sample Solar Cell

This figure (5.16) is plotted in MATLAB and the code is given in appendix 2.

5.11. Discussion

Reference cell and it's placement on the jig is very important because changing the vertical position of the cell on the platform could change the efficiency. Although most of the performance parameters of theoretical and experimental study are almost to the same but it has been observed that some discrepancies exist between these efficiencies. In our theoretical treatment, zero series resistance is considered but in experimental study, it has been found that the series resistance is 0.495 ohm. Again, there is a large variation of short circuit current density and reason behind this discrepancy is zero loss for reflection and grid coverage are treated, but in a practical cell, sun simulator counted these loss factors. Again, open circuit voltages obtained from both types of study are almost equal and it greatly depends on the reverse saturation current density which depends on the material properties.

In this model no attempt has been made to account for the effect of thickness in short circuit current density equation which is principally responsible for the observed discrepancy. It has been concluded that, this model would be useful for silicon solar cell performance parameter approximation if thickness is incorporated with short circuit current density equation.

References

[1] Rolf Stangl. 2009. Specific Characterization Method , Surface Photovoltage. *Silicon Photovoltaic,* pp.1-3.

[2] Dieter K Schroder. 2001. Surface voltage & surface photovoltage: history, theory and applications. *Meas. Sci. Technol*. 12, pp.16–31.

[3] K. Kirilov, V. Donchev, Tsv. Ivanov, K. Germanova, P. Vitanova, P. Ivanova. 2005. A surface photovoltage spectroscopy system used for minority carrier diffusion length measurements on floating zone silicon. *Journal of Optoelectronics and Advanced Materials,* vol. 7, No. 1, pp. 533 – 536.

[4] Solar Cell Physics: Recombination and generation [Motion picture]. (2011). Indiana, USA: NanoHUB.org.

[5] *Md. Abdur Rafiq Akand, Md. Rakibul Hasan, Mohammad Khairul Basher, and Mahbubul Hoq,"*
Study of Surface Photo voltage for monocrystalline silicon solar cell fabricated at BAECsolar cell lab", International Journal of Innovation and Applied Studies , ISSN 2028-9324 Vol. 7 No. 4 Aug. 2014, pp. 1479-1484

[6] K3000 LAB Solar Cell I-V Measurement System. (n.d.). Retrieved December 20, 2014, from mcscience.com/bbs/bbs/board.php?bo_table=en_product_01&wr_id=7

Chapter 6

Conclusion

In this thesis paper two types of optical characterization measurements were done successfully. One was minority carrier diffusion length and calculates the minority carrier lifetime by SPV and other was efficiency measurement. SPV measurement instrument provided by Institute of Electronics, Atomic Energy research Establishment, Savar, Dhaka and sun simulator provided by Bangladesh Council of Scientific and Industrial Research (BCSIR). The main advantage of SPV instrument is low cost.

The minority carrier lifetime is a very important parameter to explain the quality of solar cell. The lifetime can be as high as 1 milisecand the minority carrier diffusion length range is 100-300 μm [11] for silicon. We observed that diffusion length sometimes small valued. It happened due to recombination. Recombination occurs in many reasons. Doping causes defects and more recombination. Again solar grade silicon wafer (purity six nines) also provide some defects in the base region. So there need a tradeoff between excessive doping in order to increase the diffusion length and lifetime.

The efficiency of solar cell is measured by sun simulator. The drawback of this system is maintenance, contact problem and cost. The contact probes are pin type that is useful for thin film solar cell. But we have used this instrument for crystalline solar cell efficiency measurements. To use this we have cut the cell into 2cm/2cm size. Result sounds good when we compare with another sun simulator operated by LIV software.

In future these characterization instruments can help easily to measure the imported cells performances.

APPENDIX

APPENDIX 1

Sun Simulator

The sun simulator is essentially a solar cell I-V measurement system that consists of multiple components such as the K201 solar simulator, K101 photovoltaic power meter, K401 solar simulator power supply, K202 auto controller, K901 sample mounting jig and K730 the software that measures the IV characteristics. The specifications of these models are given in tables 1, 2 and 3.

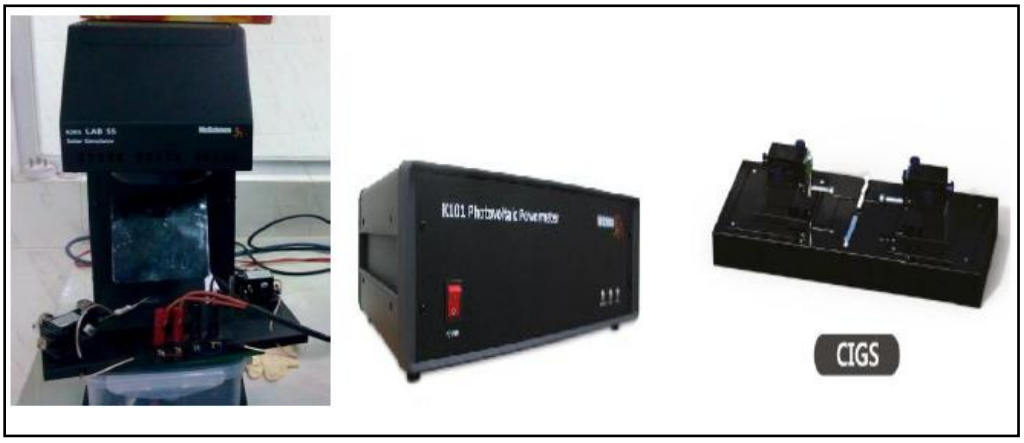

Image 1:Individual components: K201, K101 and K901 (left to right).

Table 1. Specifications for solar simulator K201

Specifications	Value
Class	AAA
Irradiance Area	25 m^2 ~ 330 m^2
Intensity	0.8 ~ 1.2 Sun
Lamp	Xenon or Metal Halide Lamp

Table 2. Specifications for photovoltaic power meter K101

Specifications	Value
Power type	DC/Pulse Electrical Power Source / Meter
Operation type	Constant Current / Voltage Operation
Voltage range	-10 ~ +10V
Current range	1 A or 10 A or 20 A (User Selectable)
Sweep type	Automatic I-V Sweep
Input type	Reference Cell / Photodiode Input

Table 3. Specifications for auto controller K202 .

Specifications	Value
Calibration	Auto intensity to 1 Sun
Ari mass filter auto control	AM 0 to AM 1.5
Optical shutter control	Auto

Table 4. Specifications for Lamp Power Supply (K401)

Specifications	Value
Power Source for Xe Lamp Operation	150 W ~ 4 kW
Protection	UVP, UCP, OVP, OCP
Ignitor Control Signal	
Shutter Control Signal	
Operation Time Count:	

APPENDIX-2

Specification for K730 Solar Cell I-V Test Software

Table 5. Specification for K730 Solar Cell

MS Windows XP or Windows 7 OS
Test Condition Editing & Recipe Management
CSV Format Data File
Real Time Voltage, Current, Power and Temperature Monitoring
Manual/Automatic Scan Range
Scan Direction Select
Data Point Setting
Scan Speed Setting
1 Sun Calibration Function
Data Correction using Reference Monitoring
Automatic Parameter Output
Isc Monitoing Function
Series Resistance and Shunt Resistance

APPENDIX-3

1. MathLAB code for SPV curve

```
clc;
clearall;
closeall;
a=[  1.05E-01   114.2595978
2.00E-01    89.04719501
3.22E-01    98.32841691
4.76E-01    61.09108681
6.76E-01    9.98851321
9.01E-01    87.65778401
1.14E-01    88.09020437
1.42E+00    101.0713564
1.73E+00    83.12551953
2.05E+00    60.61708189
2.42E+00    105.7529611
2.84E+00    103.1991744
3.29E+00    102.817191
3.88E+00    92.09799226
4.52E+00    61.97706848
5.26E+00    37.37619137
6.02E+00    17.45992946
7.04E+00    9.23463357
8.40E+00    6.209598798
9.90E+00    4.050829812
1.18E+01    3.202674874
1.41E+01    2.924814713
1.69E+01    2.3976618
2.08E+01    3.621115448
2.61E+01    4.610547088
3.27E+01    7.532672969
4.17E+01    9.232843069
5.46E+01    6.706413343
7.46E+01    11.45908534
1.04E+02    14.31926227
1.56E+02    9.367330498      ];
a1=a(:,1);
a2=a(:,2);
plot(a1,a2, 'b');

b=[  8.40E+00   6.209598798
4.17E+01    9.232843069
7.46E+01    11.45908534
-90         0.65      ];
b1=b(:,1);
b2=b(:,2);
holdon, plot(b1,b2,'b');
xlabel('Reciprocal of Penetration depth (1/alpha)');
ylabel('Reciprocal of SPV (1/Vspv)');
```

2. Matlab code for I-V characteristic curve

```
clc;
clearall;
closeall;
a=[ -0.065  617.745
-0.057  578.861
-0.049  594.281
-0.042  617.447
-0.037  602.449
-0.029  575.118
-0.022  613.33
-0.014  616.895
-0.009  584.613
-0.002  588.218
0.006   615.539
0.013   609.631
0.018   573.632
0.026   605.436
0.034   616.03
0.041   593.335
0.046   578.358
0.054   615.494
0.061   615.211
0.069   578.296
0.074   593.123
0.082   614.749
0.089   603.001
0.097   571.632
0.102   607.19
0.109   612.588
0.117   585.694
0.125   578.274
0.129   610.486
0.137   610.411
0.145   569.633
0.149   589.723
0.157   605.969
0.164   592.839
0.172   562.767
0.177   600.126
0.185   600.186
0.192   571.754
0.2     565.329
0.205   593.866
0.212   590.766
0.22    548.825
0.228   565.844
0.233   580.317
0.24    564.923
0.248   532.813
0.255   564.034
0.259   563.16
0.268   532.934
```

```
0.275   523.154
0.282   544.737
0.287   540.281
0.295   499.198
0.303   510.295
0.31    517.983
0.315   503.374
0.323   469.847
0.329   493.081
0.337   486.759
0.343   460.534
0.35    444.966
0.357   459.87
0.365   449.705
0.37    415.772
0.377   417.682
0.385   420.163
0.393   403.139
0.398   373.278
0.405   385.247
0.412   377.267
0.42    352.165
0.425   334.989
0.433   343.054
0.44    330.883
0.448   299.715
0.452   296.217
0.46    295.566
0.468   279.634
0.473   253.067
0.479   254.488
0.487   244.673
0.494   224.976
0.5     206.855
0.507   206.521
0.515   192.118
0.522   169.134
0.527   159.439
0.534   153.275
0.542   137.953
0.55    114.678
0.555   109.197
0.562   97.71
0.569   81.512
0.577   62.262
0.582   55.585
0.589   40.027
0.597   21.986
0.605   7.024
0.609   -0.901
0.616   -15.18       ];
a1=a(:,1);
a2=a(:,2);
plot(a1,a2, 'r');
legend('Current (mA)');

b=[ -0.065  -39.968
```

-0.057	-32.767
-0.049	-29.2
-0.042	-26.109
-0.037	-22.099
-0.029	-16.799
-0.022	-13.524
-0.014	-8.801
-0.009	-5.246
-0.002	-1.25
0.006	3.483
0.013	7.814
0.018	10.389
0.026	15.677
0.034	20.746
0.041	24.415
0.046	26.86
0.054	32.991
0.061	37.764
0.069	39.999
0.074	43.979
0.082	50.176
0.089	53.535
0.097	55.199
0.102	61.657
0.109	66.782
0.117	68.591
0.125	72.043
0.129	78.907
0.137	83.458
0.145	82.493
0.149	88.157
0.157	95.113
0.164	97.481
0.172	96.917
0.177	105.966
0.185	110.835
0.192	110.034
0.2	112.846
0.205	121.5
0.212	125.28
0.22	120.657
0.228	128.803
0.233	134.988
0.24	135.452
0.248	132.066
0.255	143.668
0.259	146.075
0.268	142.714
0.275	144.004
0.282	153.846
0.287	155.278
0.295	147.356
0.303	154.445
0.31	160.48
0.315	158.618
0.323	151.564
0.329	162.436

```
0.337   163.99
0.343   157.736
0.35    155.728
0.357   164.381
0.365   164.107
0.37    153.795
0.377   157.622
0.385   161.698
0.393   158.284
0.398   148.535
0.405   155.937
0.412   155.526
0.42    147.809
0.425   142.477
0.433   148.47
0.44    145.469
0.448   134.192
0.452   134.009
0.46    135.831
0.468   130.773
0.473   119.688
0.479   122.024
0.487   119.222
0.494   111.235
0.5     103.371
0.507   104.747
0.515   98.877
0.522   88.364
0.527   84.093
0.534   81.892
0.542   74.779
0.55    63.055
0.555   60.585
0.562   54.912
0.569   46.393
0.577   35.921
0.582   32.346
0.589   23.579
0.597   13.129
0.605   4.247
0.609   -0.549
0.616   -9.358       ];

b1=b(:,1);
b2=b(:,2);
holdon, plot(b1,b2,'g');
legend('Power (mW)');
xlabel('Voltage (V)');
ylabel('Current (mA) & Power (mW)');
legend('Current (mA)', 'Power (mW)');
```